2004). Those studies characterized the pathological changes such as the appearance of oncocytic hepatocytes, cytomegalic hepatocytes and bile duct hyperplasia in the subacute phase. In the acute phase, SZ induced several hepatic changes including lipid peroxidation, mitochondrial swelling, peroxisome proliferation and inhibition of hepatocyte proliferation before the elevation of the serum glucose levels (Kume et al., 2004). We also analyzed molecular genetic changes in the liver before and after the induction of hyperglycemia using the Affymetrix GeneChip. Many of the up-regulated genes were categorized into cell cycle/apoptosis-related genes, immune/allergy-related genes and stress response/xenobiotic metabolism-related genes. On the other hand, genes related to glucose, lipid and protein metabolisms were down-regulated (Kume et al., in press). These morphological and genetic changes occurred before the induction of hyperglycemia. Therefore, it is suggested that those changes were attributable to the direct effects of SZ on hepatocytes rather than the secondary effects of diabetes or hyperglycemia.

Several reports have focused on the toxic mechanisms of SZ in islet cells in vitro (Ledoux and Wilson, 1984; Flament and Remacle, 1987; Eizirik et al., 1993; Turk et al., 1993; Bellmann et al., 1995), however, no researchers reported detailed changes in SZ-treated hepatocytes in vitro. Morphological examinations and gene expression analysis were performed on the SZ-treated mouse primary hepatocytes to clarify direct effects of SZ on hepatocytes.

Materials and methods

The study was approved by the Ethical Committee at Tanabe Seiyaku Co. Ltd., and all efforts were made to minimize animal suffering.

Animals

Two 8-week-old male Crj:CD-1(ICR) mice (Charles River Japan Inc., Kanagawa, Japan) were used.

Primary cultured hepatocytes

Hepatocytes were isolated from the mice with use of collagenase perfusion under pentobarbital anesthesia. The isolated hepatocytes were seeded at a density of 1.0×10^6 cells per 35 mm dish in 2 mL medium (William's E medium containing 5% FCS, 0.1 μM dexamethasone, 6.25 μg/mL insulin, 6.25 ng/mL transferrin, 6.25 ng/mL selenium, 100 U/mL penicillin, 100 μg/mL streptomycin, and 50 μg/mL Matrigel). At 24 h after seeding, SZ was applied on the hepatocytes within the same medium for 6 or 24 h at 37 °C. Applied concentrations were selected as 0, 1, 3, 10, 30 and 100 mM. In all 4, 2, and 2 dishes of each concentration were provided for an analysis of cell survival rate, electron microscopic examination, and GeneChip analysis, respectively. Phase contrast micrographs were taken from the dishes for electron microscopic examination.

Cell survival rate (WST-1 assay)

After the 6 or 24 h-incubation with SZ, WST-1 (Wako Pure Chemical Industries Ltd., Osaka, Japan) was added for each dish at a final concentration of 15%, and the dish was incubated for another 3 h. Following the incubation, absorbance was read at a wavelength of 450 nm using a spectrophotometer (Bio-Rad Laboratories Inc., CA, USA). Percentage of survival cell was calculated using the following formula: (absorbance of treated dish/absorbance of control dish) × 100. For the calculation of the 50% inhibition concentration (IC50) value, concentration-response data were fit by non-regression analysis to sigmoid curves by using the GraphPad Prism program (GraphPad Software Inc., CA, USA).

Morphological examination

After the phase contrast micrographs were taken, hepatocytes were fixed with 2.5% glutaraldehyde and 2.0% formaldehyde, postfixed with 1% osmium tetroxide, and embedded in epoxy resin. Semithin sections were stained with toluidine blue and observed under a light microscope. Ultrathin sections were doubly stained with uranyl acetate and lead citrate and observed under a JEOL-1210 electron microscope (JEOL Co. LTD., Tokyo, Japan).

RNA extraction

Total RNA was isolated as the manual of QIAGEN RNEASY kit (QIAGEN, CA, USA). For lysis of cells and tissues before RNA isolation, Buffer RLT with β-mercaptoethanol was added and incubated for 10 min at 37 °C. Total RNA was extracted by using QIAshredder spin column and RNeasy mini spin column. Absorbance rate of the sample at 260 nm/280 nm was determined.

Affymetrix GeneChip analysis

Total RNA was labeled as described in the GeneChip Expression Analysis Technical Manual (Affymetrix, CA, USA). mRNA was reverse-transcribed into cDNA using SuperScript Choice system (Invitrogen, Tokyo, Japan) and T7-(dT)24 primer (Amersham Biosciences, NJ, USA). The cDNA was converted to labeled cRNA using Bioarray HighYield RNA Transcript Labeling Kit

(Affymetrix), which was purified using RNeasy Mini Kit (QIAGEN). The labeled cRNA was hydrolyzed in fragmentation buffer (40 mM Tris-acetate pH8.1, 100 mM KOAc, 30 mM MgOAc) to a size of approximately 35–200 nucleotides.

Ten microgram of the fragmented cRNA was hybridized with the Murine Genome U74AV2 array (Affymetrix) in hybridization cocktail (0.05 ug/uL cRNA, 50 pM control oligonucleotide B2, 1.5 pM bioB, 5 pM bioC, 25 pM bioD, 100 pM cre, 0.1 mg/mL herring sperm DNA, 0.5 mg/mL acetylated BSA, 100 mM MES, 1 M Na+, 20 mM EDTA, 0.01% Tween20). Hybridization was carried out overnight (16 h) at 45 °C, followed by washing, and staining with streptavidin-phycoerythrin (SAPE, Molecular Proves, OR, USA). Hybridization assay procedures including preparation of solutions were carried out as described in the Affymetrix GeneChip Expression Analysis Technical Manual. The distribution of fluorescent material on the array was determined using a confocal laser scanner (GeneArray Scanner, Affymetrix).

Array data processing

Signal quantification, background adjustment, judgment of detection call and other analysis were performed using the Microarray Suite (MAS) ver. 5.0 (Affymetrix). All arrays were globally scaled to a target value of 200. Genes were only considered for further analysis, if their corresponding probe sets had a signal intensity over 300 and their detection call were P (present). Pair-wise comparison analysis was performed between SZ-treated hepatocytes and control hepatocytes. The signal log ratio (SLR) was calculated for each probe set using the following formula: $\log_2$ (signal intensity in SZ-treated mice/that in control mice). Probe sets with SLR greater or equal to 1.0 was judged as 'up-regulated'. On the other hand, probe sets with SLR less or equal to −1.0 was judged as 'down-regulated'.

Annotation information on the probe sets on the U74A V.2 array was downloaded from the NetAffyx provided by Affymetrix. The probe sets judged as 'up-regulated' or 'down-regulated' were categorized according to the annotation information and protein information from Protein Knowledgebase provided by Swiss Institute of Bioinformatics (Swiss-Prot).

Results

Cell survival

Fig. 1 shows the concentration–response curve of the cell survival analysis. IC50 value in 6 h exposure was 62 mM and that in 24 h exposure was 7 mM.

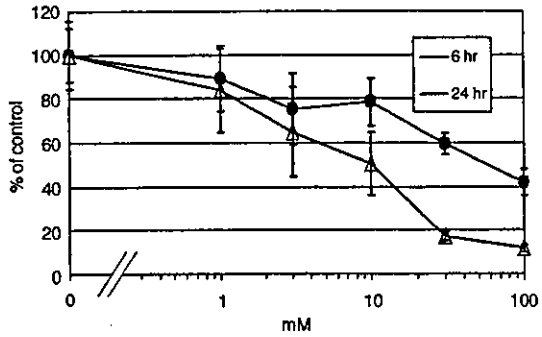

Fig. 1. Cell survival rate of mouse primary cultured hepatocytes exposed with SZ. Closed circle expressed the concentration–response curve of 6 h exposure, and open triangle expressed the one of 24 h exposure. The 50% inhibition concentration (IC50) values were approximately 62 and 7 mM at 6 h exposure and 24 h exposure, respectively.

Morphological examination

Apparent differences were not observed under the phase contrast microscope between the SZ-treated hepatocytes and the control hepatocytes. Only slight decrease in the cell density was observed in 100 mM-24 h exposure group.

Light microscopic analysis using semi-thin toluidin blue stained sections was performed on 1–10 mM exposure groups. Margination of nuclear chromatin was observed in the hepatocytes treated with SZ for 24 h at doses of 3 and 10 mM (Fig. 2). No other changes were observed.

Compaction and margination of nuclear chromatin in the SZ group were also observed under the electron microscope (Fig. 3). Some hepatocytes in the SZ group showed increases in lipid droplets, lysosome and peroxisome, and the structure of crista of some mitochondria were obscure, although most hepatocytes showed no apparent difference in the cytoplasm.

GeneChip analysis

Comparison analysis of the expression profiles was performed between SZ-treated hepatocytes and control hepatocytes. Time points and concentrations were 1 mM-6 h, 1 mM-24 h and 3 mM-24 h exposure. Table 1 shows the number of the up-regulated (SLR > = 1.0) or the down-regulated (SLR < = −1.0) probe sets. The number of up-regulated probe sets were 16, 18 and 210, respectively. The number of down-regulated probe sets were 30, 20 and 278, respectively. Probe sets, of which SLR was over 1.5 or was under −1.5, were picked up and tabulated in Table 2. The

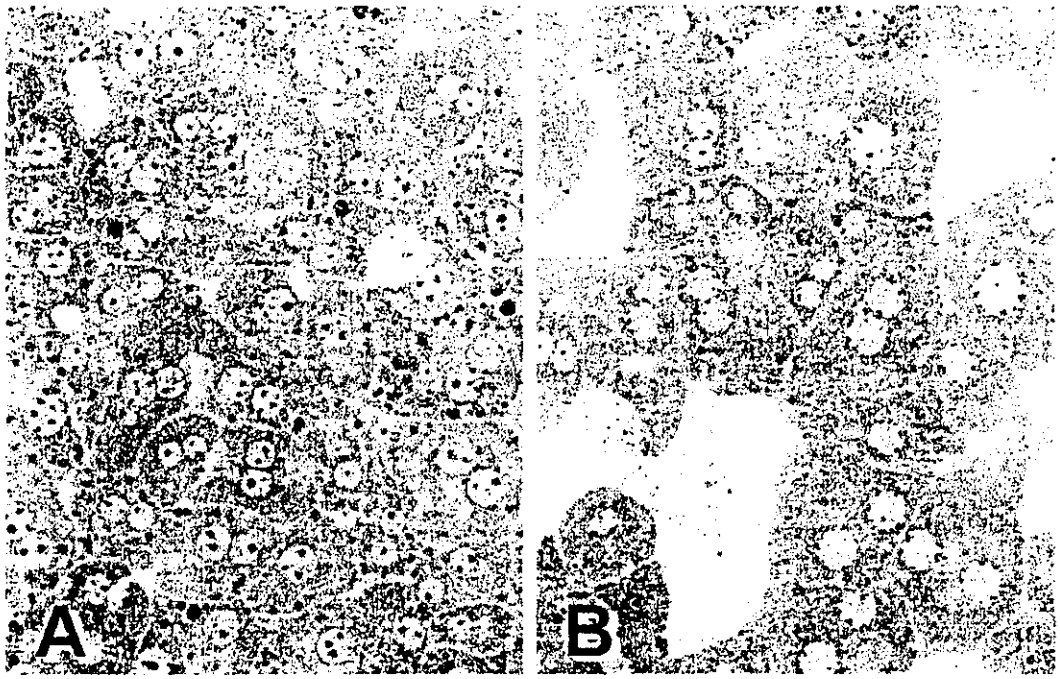

Fig. 2. Light microphotographs of primary cultured hepatocytes treated with vehicle (A) or 10 mM of SZ (B) for 24 h. Marked chromatin margination was observed in nuclei of the hepatocytes treated with SZ. Toluidin blue, × 500.

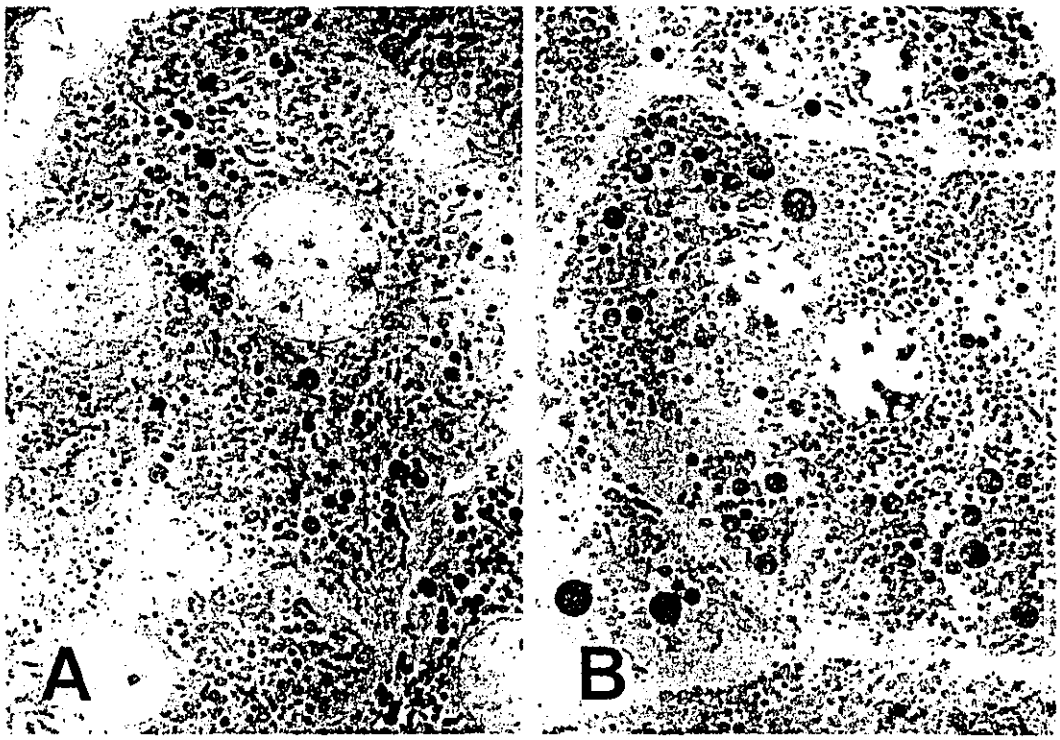

Fig. 3. Electron microphotographs of primary cultured hepatocytes treated with vehicle (A) or 10 mM of SZ (B) for 24 h. Compaction and margination of nuclear chromatin were observed in nuclei of the hepatocytes treated with SZ, × 1800.

Table 1. Number of up- or down-regulated genes in the primary cultured hepatocytes exposed to SZ

	1 mM 6 h	1 mM 24 h	3 mM 24 h
Up-regulated genes	16	18	210
Down-regulated genes	30	20	278

Up-regulated genes: signal $\log_2$ ratio to the control (SLR) > = 1.0. Down-regulated genes: signal $\log_2$ ratio to the control (SLR) < = −1.0.

regulated genes showed a broad range, but many of the up-regulated genes were categorized into cell cycle/apoptosis-related genes and stress response/xenobiotic metabolism-related genes. 'Growth arrest and DNA-damage-inducible 45' (GADD45), 'p53 apoptosis effector related to Pmp22' (perp), 'tumor necrosis factor receptor superfamily, member 6' (tnfrsf6) and 'RAD51-like 1' (Rad51l1) were of particular note. On the other hand, many of the down-regulated genes belonged to glucose, lipid and protein metabolism-related genes or immune/allergy related genes. '3-hydroxy-3-methylglutaryl-Coenzyme A synthase 1' (Hmgcs1), 'microsomal triglyceride transfer proteine' (Mttp), 'stearoyl-Coenzyme A desaturase 2' (Scd2) and other lipid metabolism-related genes were of particular note.

Discussion

Morphological examinations and gene expression analysis were performed on mouse primary hepatocytes exposed to SZ to clarify direct effects of the compound on hepatocytes.

IC50 value for cell survival at 6 and 24 h exposure were 62 and 7 mM, respectively, which were relatively higher values than other medical drugs, such as cisplatin, erythromycin, amiodarone, chlorpromazine, and so on, in similar evaluations using rat primary hepatocytes (Wang et al., 2002). We can say that SZ has weak direct cytotoxicity. SZ showed stronger cytotoxicity in tumor cell lines than in hepatocytes, approximately 1 mM in insulinoma cell line (Ledoux and Wilson, 1984), and around 0.4 mM in mouse lymphoma (Bhuyan, 1970).

Morphological examination revealed compaction and margination of nuclear chromatin, which were characteristics of early stage apoptosis. However, the apparent characteristics of apoptosis, i.e., nuclear fragmentation, cytoplasmic shrinkage or blebbing of the cell membrane, were not observed in this study. Those histopathological characteristics of apoptosis were not observed in SZ-treated mice (Kume et al., 2004). It is interesting that apoptosis-related genes were up-regulated both in vivo (Kume et al., in press) and in vitro, although the apparent apoptosis were not observed neither in vitro nor in vivo. Flament and Remacle (1987) reported ultrastructural changes observed in SZ-treated pancreatic islets in vitro. The changes were a slight increase in heterochromatin, swelling of nuclear membrane, dilatation of rough endoplasmic reticulum, and mitochondrial destruction, suggesting necrosis but not apoptosis. The mechanisms involved in islet cell damage and hepatocytes damage might be quite different.

Mitochondrial swelling is one of the characteristic morphological changes observed at 6 h after SZ treatment (Kume et al., 2004), which may be related to mitochondrial proliferation observed in the subacute or chronic phase (Kume et al., 1994a, b). In this study, mitochondria of some hepatocytes showed abnormal obscure crista, which might be related to mitochondrial damage, but no other mitochondrial changes were observed in vitro. Thus, we could not offer proof that the mitochondrial changes were a direct effect of SZ. However, there is some possibility that changes in mitochondrial morphology were difficult to detect in vitro in this study, because the mitochondrial shapes in vitro varied too much to differentiate a small change. Functional assays should be performed to clarify the direct effect of SZ on liver mitochondria.

Gene expression analysis revealed similar regulations of gene expression by SZ in in vivo (Kume et al., in press) and in vitro treatment, such as the up-regulation of cell cycle/apoptosis-related genes, the down-regulation of glucose, lipid and protein metabolism-related genes, and so on. Table 3 shows the in vivo and in vitro comparison, in which probe sets were picked up if their SLR were over 1.5 or were under −1.5 at representative time points (in vivo: 200 mg/kg 24 h after the administration, in vitro: 3 mM-24 h).

Among the up-regulated cell cycle/apoptosis-related genes, several major genes related to induction of cell cycle checkpoint and arrest were observed. These included growth arrest and DNA-damage-inducible 45 (GADD45), and cyclin-dependent kinase inhibitor 1A (Cdkn1a, p21). Cell cycle arrest was observed in vivo by immunohistochemical analysis, in which the ratio of the proliferating cell nuclear antigen (PCNA) positive hepatocytes was low at 24 and 48 h after the SZ-treatment (Kume et al., 2004). If we use a highly proliferative cell line rather than primary cultured hepatocytes, a decrease in cell proliferation may be observed in vitro as seen in other studies (Bhuyan, 1970; Capucci et al., 1995). Several genes related to induction of apoptosis were also up-regulated, which include 'Bcl2-associated X protein' (bax), 'apoptotic protease activating factor 1' (Apaf1), 'tumor necrosis factor receptor superfamily, member 6' (tnfrsf6), 'wild-type p53-induced gene 1' (wig1), 'transformed mouse 3T3 cell double minute 2' (mdm2) and 'p53 apoptosis effector

Table 2. Gene expression in primary cultured hepatocytes exposed with SZ

Title	GeneName	1 mM 6 h	1 mM 24 h	3 mM 24 h	Affy ID
Carbohydrate and lipid metabolism					
Cytosolic acyl-CoA thioesterase 1	Cte1	-0.2	0.9		103581_at
Cytochrome P450, 51	Cyp51	-0.2	-0.9	-1.7	94916_at
Fatty acid binding protein 1, liver	Fabp1	0.4	0		94075_at
Glucokinase	Gck	0	-0.8	-1.9	102651_at
3-hydroxy-3-methylglutaryl-Coenzyme A synthase 1	Hmgcs1	-0.6	-0.7	-1.5	94325_at
Isopentenyl-diphosphate delta isomerase	Idi1	0.1	-0.8	-1.5	96269_at
Microsomal triglyceride transfer protein	Mttp	-0.3	-0.1	-1.7	104448_at
NAD(P) dependent steroid dehydrogenase-like	Nsdhl	-0.6	-1	-2.2	93868_at
Pyruvate kinase liver and red blood cell	Pklr	-0.1	-0.5	-1.8	101471_at
Pyruvate kinase liver and red blood cell	Pklr	0.1	-0.4	-1.8	101472_s_at
Phosphomannomutase 1	Pmm1	0.2	0.6		93360_at
Stearoyl-Coenzyme A desaturase 2	Scd2	-0.2	-0.8	-1.7	95758_at
Solute carrier family 2 (facilitated glucose transporter), member 2	Slc2a2	0	-0.3	-2.2	103357_at
Protein/amino acid metabolism					
Ankyrin 3, epithelial	Ank3	-0.4	-0.7	-1.9	98477_s_at
Archain 1	Arcn1	-1.9	0.6	-0.2	94512_f_at
Arginase 1, liver	Arg1	-0.1	-0.5	-1.9	93097_at
Dopa decarboxylase	Ddc	-0.2	-0.1	-2.5	160074_at
Ubiquitin-conjugating enzyme E2E 3, UBC4/5 homolog (yeast)	Ube2e3	0.5			93033_at
Cell cycle/apoptosis					
Cyclin F	Ccnf	0.2	0.4		99073_at
Cyclin G1	Ccng1	0.2			160127_at
Growth arrest and DNA-damage-inducible 45 beta	Gadd45b	0.4	0.6		102779_at
Kinesin family member 2C	Kif2c	-0.3	0.9		160755_at
Lysyl oxidase	Lox	-1.5	0.3	0	161177_f_at
Moloney leukemia virus 10	Mov10	-0.2	-0.5	-1.5	103025_at
Myeloblastosis oncogene-like 1	Mybl1	0.2	0.6		92902_at
p53 apoptosis effector related to Pmp22	Perp	0	0.7		97825_at
Protein inhibitor of activated STAT 3	Pias3	0.7	0.8		160615_at
RAD51-like 1 (S. cerevisiae)	Rad51l1				103944_at
SH3-domain GRB2-like B1 (endophilin)	Sh3glb1	0.3	-0.8	-1.8	103569_at
Serum-inducible kinase	Snk	0.9	0.7		92310_at
Serine/threonine kinase 6	Stk6	0.3	0.4		92639_at
Tumor necrosis factor receptor superfamily, member 6	Tnfrsf6	0.6	0.6		102921_s_at
Immune and inflammation					
Activated leukocyte cell adhesion molecule	Alcam	-0.4	-0.5	-2	104407_at
Amine oxidase, copper containing 3	Aoc3	0.4	0.4		102327_at
Chemokine (C-C motif) ligand 2	Ccl2	0.2	-0.9	-2.4	102736_at
Chemokine (C-C motif) ligand 7	Ccl7	0.3	-1	-1.9	94761_at
CD47 antigen (Rh-related antigen, integrin-associated signal transducer)	Cd47	0.2	-0.3	-1.5	103611_at
Complement component factor h	Cfh	-0.2	-0.6	-1.5	94743_f_at
Decay accelerating factor 1	Daf1	-2.5	0.2		103617_at
Insulin-like growth factor binding protein 1	Igfbp1	-0.2	-0.7	-1.6	103896_f_at
Lipopolysaccharide binding protein	Lbp	0.1	-0.5	-1.8	96123_at
Mannan-binding lectin serine protease 1	Masp1	-0.6	-0.4	-2	102284_at
Serum amyloid A 4	Saa4	0.3	0.2		92242_at
Thromboxane A synthase 1, platelet	Tbxas1	0.6			162136_r_at
Stress response and xenobiotic metabolism					
ATP-binding cassette, sub-family B (MDR/TAP), member 1B	Abcb1b	0.5	0		93414_at
Aldo-keto reductase family 1, member C6	Akr1c6	0.1	0.4		92556_at
Ceruloplasmin	Cp	-0.1	-0.8	-2	92851_at
Heat shock transcription factor 4	Hsf4	0	0.3		100384_at
Heat shock protein 1A	Hspa1a	0.3	0.3		93875_at
heat shock protein 1B	Hspa1b	-0.3	0.3		100946_at
Lactotransferrin	Ltf	0.7			101115_at
Solute carrier family 11 (proton-coupled divalent metal ion transporters), member 2	Slc11a2	-0.1	-0.5	-2.1	104451_at
Sulfotransferase family 1A, phenol-preferring, member 1	Sult1a1	-0.4	-0.8	-2	103087_at

Table 2. *(continued)*

Title	GeneName	1 mM 6 h	1 mM 24 h	3 mM 24 h	Affy ID
Cytoskelton etc.					
Cadherin 2	Cdh2	0.1	-0.2	-1.8	102852_at
Gap junction membrane channel protein alpha 1	Gja1	-0.2	0.2		100065_r_at
Gap junction membrane channel protein beta 2	Gjb2	-0.2	-0.4	-2.1	98423_at
Gephyrin	Gphn	-0.9	0.1	-2.1	99441_at
Microtubule-actin crosslinking factor 1	Macf1	-1.7	0.3	0.1	98402_at
Microtubule-associated protein 4	Mtap4	0.1	-1	-1.6	92795_at
Par-3 (partitioning defective 3) homolog (C. elegans)	Pard3	-0.8	-0.3	-1.5	160607_at
p300/CBP-associated factor	Pcaf	0.2	-0.6	-1.8	161116_at
Ryanodine receptor 3	Ryr3	-0.6	-2.3	-2.5	97126_at
Stathmin 1	Stmn1	0.3	0.2		97909_at
Utrophin	Utrn	-1.4	-0.5	-1.7	92507_at
Miscellaneous					
Betacellulin, epidermal growth factor family member	Btc	-0.3	-1.7	-0.9	95310_at
Creatine kinase, mitochondrial 1, ubiquitous	Ckmt1	-0.8	-0.3		160565_at
Procollagen, type IV, alpha 5	Col4a5	0.2	0	-2.2	93220_at
Cysteine rich protein 2	Crip2	0.3	0.4		101593_at
C-terminal binding protein 2	Ctbp2	-0.2	0	-3.8	160979_at
Fibroblast growth factor 1	Fgf1	0.2	-0.5	-1.7	100494_at
Fibroblast growth factor 7	Fgf7	0.1	-0.1	-1.9	99435_at
Gastric intrinsic factor	Gif	-0.2			92690_at
Homeo box A9	Hoxa9	-2	-0.7	0.4	92745_at
Hydroxysteroid (17-beta) dehydrogenase 2	Hsd17b2	0	-0.6	-1.5	101891_at
Inositol 1,4,5-triphosphate receptor 5	Itpr5	-1	-0.4	-1.7	101441_i_at
Male enhanced antigen 1	Mea1	0.5		0.6	94890_at
Matrix metalloproteinase 15	Mmp15		0.9		93612_at
Nemo like kinase	Nlk	-0.6	-0.4	-2.4	93935_at
Expressed in non-metastatic cells 4, protein	Nme4	-0.1	0.9		160473_at
Nicotinamide nucleotide transhydrogenase	Nnt	-0.1	-0.4	-1.7	99009_at
Paired box gene 6	Pax6	-0.4			92271_at
Protein phosphatase 2, regulatory subunit B (B56), delta isoform	Ppp2r5d				101875_at
DNA primase, p58 subunit	Prim2	0	-0.6	-3.2	95549_at
Platelet-activating factor receptor	Ptafr	-0.5	0.7		94158_f_at
Reelin	Reln	-2.6	-1.4	-1.7	96591_at
Serine (or cysteine) proteinase inhibitor, clade E, member 1	Serpine1	-0.5	-0.1	-1.9	94147_at
Serine (or cysteine) proteinase inhibitor, clade E, member 2	Serpine2	0.6			97487_at
Serine (or cysteine) proteinase inhibitor, clade F, member 2	Serpinf2	-0.2	-0.4	-1.8	101928_at
Splicing factor, arginine/serine-rich 1 (ASF/SF2)	Sfrs1	0.1	0.1	-2.5	160141_r_at
Sialyltransferase 9 (CMP-NeuAc:lactosylceramide alpha-2,3-sialyltransferase)	Siat9	-0.4	-0.6	-1.8	98596_s_at
Solute carrier family 25 (mitochondrial carrier; adenine nucleotide translocator), member 4	Slc25a4	0.3	-0.4	-1.5	93084_at
Small proline-rich protein 1B	Sprr1b	-0.2			100445_f_at
Endothelial-specific receptor tyrosine kinase	Tek	-1.5	0.2	0.6	102720_at
Troponin C, cardiac/slow skeletal	Tncc	0.4	0.4		101063_at
Urate oxidase	Uox	-0.1	-0.5	-2	92606_at

Data is shown as signal $\log_2$ ratio to each control group.

related to Pmp22' (perp). Thus, the activation of apoptosis should be envisioned. These expression changes should be related to the compaction and margination of nuclear chromatin.

Many genes related to lipid and glucose metabolism were down-regulated. Some of the fatty acid synthesis-related factors, 'stearoyl-CoA desaturases' (Scd1, Scd2) and 'fatty acid syhthase' (fasn), and cholesterol synthetase, '3-hydroxy-3-methylglutaryl-Coenzyme A synthase 1' (Hmgcs1) were down-regulated. 'Mttp', which transfers lipids onto the apoB polypeptide in the endoplasmic reticulum (Raabe et al., 1999), was also down-regulated. We observed similar results in vivo (Kume et al., in press). These findings may not indicate that SZ controls these parameters directly, but may indicate that the energy for the lipid and glucose metabolism was not supplied due to the hepatocyte injury.

Most of the genes related to the stress-response and xenobiotic metabolism such as 'RAD51-like 1' (Rad51l1) and 'Heat shock transcription factor 4'

Table 3. Gene expressions in primary cultured hepatocytes exposed with SZ (in vitro) and in the SZ-treated mice (in vivo)

GeneName	*in vitro* 3 mM 24 h	*in vivo* 200 mg/kg 24 h	AffyID
Carbohydrate and lipid metabolism			
Amy2	-4.4	-0.5	97529_f_at
Cps	-0.1	-2.1	160132_at
Dio1			103581_at
Cyp51	-1.7	-2.2	94916_at
Cyp8b1		-3.8	103294_at
Fabp1		-0.7	94075_at
Fasn	-0.8	+1.5	94575_at
Fdps	-1	-2	160424_f_at
Fdps	-0.8	-2.8	99066_at
Gck	-1.9	-2.4	102851_at
Hmgcs1	-1.5	-1.5	94325_at
Hmgcs2		-2.1	92500_at
Idi1	-1.5	-2.5	98766_at
Lipc	-0.8	-1.9	98982_at
Mtp	-1.7	-0.1	104448_at
Nedh1	-2.2	-1.8	93868_at
Nedh1	-1.5	-1.7	98631_g_at
Pla	-1.8	-1.2	101471_at
Pla	-1.8	-0.8	101472_s_at
Pmm1			93360_at
Pnlipp1			92901_at
Scamol	-0.3	-2	160368_at
Scd1	-0.5	-1.7	94057_g_at
Scd2	+1.7	-0.1	96756_at
Slc2a2	-2.2	-0.3	103357_at
Thrsp	0.7	-1.7	160008_at
Protein/amino acid metabolism			
Amt3	-1.9		98477_g_at
Arg1	-1.9	-0.4	93097_at
Bhmt	-0.2	-1.9	94049_at
Ceso	-0.7	-2.4	98184_at
Ddc	-2.5	-1.3	160074_at
Ela1	0.5	-1.7	95783_at
Fbxo21	-0.3	-1.7	104108_at
Gamt	0.8	-2	101408_at
Mug1	-1.2	-1.6	92637_f_at
Tat	-0.5	-1.9	96328_at
Tyr4	-1.4		101043_f_at
Ube2e3		0.2	93033_at

GeneName	*in vitro* 3 mM 24 h	*in vivo* 200 mg/kg 24 h	AffyID
Cell cycle/apoptosis			
Bax	0.8		93535_at
Btg2	0.7		101583_at
Ccnl		0.3	99073_at
Ccng1			160127_at
Cdkn1a			94981_at
Cdkn1b			96967_at
Dusp9	-1		93265_at
Ei24	0.9		99629_at
Gdf2	0	-1.3	97531_at
Gadd45b		0.9	102779_at
Krge		0.2	160755_at
Lox	0	+1.6	161177_f_at
Mdm2			98110_at
Mdm10	-1.5	-0.2	103025_at
Myt1l			92902_at
Perp			97825_at
Plau0			160615_at
Rhbgtb1	-1.8	0	103586_at
Sns			92310_at
Stx8		-0.3	92038_at
Tnfrsf8			102921_s_at
Tpd1	0.2		98532_at
Wig1	0.9		92202_at

GeneName	*in vitro* 3 mM 24 h	*in vivo* 200 mg/kg 24 h	AffyID
Stress response and xenobiotic metabolism			
Abcb1b			93414_at
Akr1c6		-0.5	92556_at
Cp	-2	-0.7	92851_at
Cyp2b9	-0.1		101842_at
Fmo3	-0.8	+1.7	104421_at
Hsf4			100384_at
Hspa1a		-0.8	93875_at
Hspb1b		-1.5	100048_at
Ltf			101115_at
Rad51l1		0.2	103944_at
Saa3	0.3		102712_at
Slc11a2	-2.1	-1.1	104451_at
Sult1a1	-2	-0.4	103067_at
Tgm1		-3.3	97402_at
Tpm2			95896_at
Immune and inflammation			
Alcam	-2		104407_at
Anc3		-0.4	102327_at
Ania	-0.3		101030_at
Ccl2	-2.4		102736_at
Ccl7	-1.9		94761_at
Cd47	-1.6	-0.2	103811_at
Cln	-1.5	0	94743_f_at
Cxcl1	-0.9		963_at
Cxcl1	-0.8		95340_g_at
Cxcl12	0.2	-1.6	100112_at
Dsf1		0.2	103617_at
Icam1	0.9		96752_at
Igbp1	-1.6	0.2	103866_f_at
Lbp	-1.6	-1.2	96123_at
Lyb2	0.5		160553_at
Masp1	-2	-0.9	102284_at
Mb2	0.7		97427_at
Mrc2	-0.4		92582_at
Pgr	0	-1.7	99926_at
S100a11	0.1		98600_at
Saa4		0.3	92242_at
Serpina6	0.3	-2.4	96227_at
Tnfaip1		-2.7	162136_f_at

GeneName	*in vitro* 3 mM 24 h	*in vivo* 200 mg/kg 24 h	AffyID
Miscellaneous			
Ahcy	-0.1	+1.6	98024_at
Alas2	-1.5	-0.2	92788_s_at
Ang	0.7		94302_f_at
Atp6v1g	0.7		99051_at
Carl1	-0.2	-1.8	94079_at
Car3	0.9	-2.3	160375_at
Car5a	0.7	-1.7	94137_at
Ccrn4l	-0.1		99535_at
Cdh2	-1.8	-0.2	102952_at
Ckm1			160505_at
Cox4i1	-2.2	-0.8	93220_at
Crot2			101540_at
Cbp2	-3.6	0.2	160879_at
Dbp	0.7		160841_at
Dio1	-0.2	-1.9	95352_at
Fgf1	-1.7	-1.4	100464_at
Fgf7	-1.9	0.4	99435_at
Gif		-0.1	97660_at
Gpt1		-0.3	100095_r_at
Gtf2	-2.1	-0.8	98423_at
Gphn	-2.1	-0.9	99441_at
Hsd17b2	-1.3	-1.3	101901_at
Igfbp2	0	-2.2	98627_at
Ifpr5	-1.7	-0.3	101441_f_at
Klk6	-1.7		100081_f_at
Lpin1	-0.4		98892_at
Mmp15		-0.2	93612_at
Mtap6	-1.6	-0.6	92705_at
Nik	-2.4	0.1	93935_at
Nme4			160473_at
Nnt	-1.7	-0.5	98009_at
Pard3	-1.5	-0.7	160807_at
Pax8		-0.2	92271_at
Pcaf	-1.8	-0.2	161116_at
Ppp2r5d		-0.2	101875_at
Prim2	-3.2	-2.1	95540_at
Prkrl		0.1	94158_f_at
Rekh	-1.7	-0.7	99581_at
Rem1	-1.7		98480_s_at
Ryr3	-2.9	-0.1	97126_at
Scrib	0.8		102808_at
Serpine1	-1.9		94147_at
Serpine2		0.8	97487_at
Serpinf2	-1.8	-0.4	101928_at
Strg1	-2.5		160141_r_at
Sult1	-1.8	0.6	98598_g_at
Slc25a4	-1.5	0.6	93084_at
Sprr1b		0.5	100445_f_at
Stmn1			97909_at
Tek	0.6		102720_at
Tnc			101060_at
Ucn	-2	-0.8	92808_at
Utrn	-1.7	0.8	92507_at

Data is shown as signal $\log_2$ ratio to each control group.

(Hsf4) were up-regulated in vitro and in vivo. However, some genes related to the stress-response such as 'heat shock proteins' (Hspa1a, 1b) were up-regulated in vitro but not in vivo. Those proteins directly related to the nuclear damages, i.e. Rad51l1 and Hsf4, might be regulated the same in vitro and in vivo, and some genes in this category, such as hspa1a and 1b, might be regulated in a more complicated manner.

The most conspicuous difference was observed in the immune/allergy related genes. In the other categories, most genes were regulated in the same direction, but many of the immune/allergy-related genes were regulated in the opposite direction between in vivo and in vitro. Most genes were up-regulated in vivo, although in vitro most were down-regulated. The reason is unknown, but it could be related to the fact that there were practically no immune cells interacting with hepatocytes in the in vitro condition.

We can see the similarity in directions for the gene expression changes in 1 mM-24 h exposure group and 3 mM-24 hr exposure group, although the magnitudes were different. Only four genes in the tabulated 95 genes were regulated in opposite directions. Therefore, we can say that the gene expression changes were dose dependent, and small changes, i.e.—$1.0 < SLR < 1.0$, should have had some meaning. We should pay attention to those small expression changes.

In conclusion, SZ induced morphological and gene expression changes in vitro. Those changes were related to apoptosis, cell proliferation, and carbohydrate and lipid metabolisms, and were similar as those observed in vivo. These results strongly support the former results; those changes, which started prior to the elevation of the serum glucose levels, were due to the direct action of SZ on the liver, rather than the secondary effect of diabetes.

Acknowledgements

We thank Ms H. Yamasaki, Ms M. Kurabe, Ms E. Ohtsuka, Ms N. Shimazu, and other members of our laboratory for their technical assistance.

Reference

Bellmann K, Wenz A, Radons J, Burkart V, Kleemann R, Kolb H. Heat shock induces resistance in rat pancreatic islet cells against nitric oxide, oxygen radicals and streptozotocin toxicity in vitro. J Clin Invest 1995;95: 2840–5.

Bhuyan BK. The action of streptozotocin on mammalian cells. Cancer Res 1970;30:2017–23.

Capucci MS, Hoffmann ME, De Groot A, Natarajan AT. Streptozotocin-induced toxicity in CHO-9 and V79 cells. Environ Mol Mutagen 1995;26:72–8.

Doi K, Yamanouchi J, Kume E, Yasoshima A. Morphologic changes in hepatocyte nuclei of streptozotocin (SZ)-induced diabetic mice. Exp Toxic Pathol 1997;49:295–9.

Eizirik DL, Bjorklund A, Cagliero E. Genotoxic agents increase expression of growth arrest and DNA damage—inducible genes gadd 153 and gadd 45 in rat pancreatic islets. Diabetes 1993;42:738–45.

Flament P, Remacle C. Ultrastructural aspects of streptozotocin cytotoxicity on rat pancreatic islets in vitro. Virchows Arch B 1987;53:107–12.

Kume E, Doi C, Itagaki S, Nagashima Y, Doi K. Glomerular lesions in unilateral nephrectomized and diabetic (UN-D) mice. J Vet Med Sci 1992;54:1085–90.

Kume E, Itagaki S, Doi K. Cytomegalic hepatocytes and bile duct hyperplasia in streptozotocin-induced diabetic mice. J Toxicol Pathol 1994a;7:261–5.

Kume E, Ohmachi Y, Itagaki S, Tamura K, Doi K. Hepatic changes of mice in the subacute phase of streptozotocin (SZ)-induced diabetes. Exp Toxic Pathol 1994b;46:368–74.

Kume E, Fujimura H, Matsuki N, Ito M, Aruga C, Toriumi W, Kitamura K, Doi K. Hepatic changes in the acute phase of streptozotocin (SZ)-induced diabetes in mice. Exp Toxic Pathol 2004;55:467–80.

Kume E, Aruga C, Takahashi K, Miwa S, Ito M, Fujimura H, Toriumi W, Kitamura K, Doi K. Gene expression profiling in streptozotocin treated mouse liver using DNA microarray. Exp Toxic Pathol, in press.

Ledoux SP, Wilson GL. Effects of streptozotocin on a clonal isolate of rat insulinoma cells. Biochim Biophys Acta 1984;804:387–92.

Raabe M, Veniant MM, Sullivan MA, Zlot CH, Bjorkegren J, Nielsen LB, Wong JS, Hamilton RL, Young SG. Analysis of the role of microsomal triglyceride transfer protein in the liver of tissue-specific knockout mice. J Clin Invest 1999;103:1287–98.

Sibay TM, Hausler HR, Hayes JA. The study and effect of streptozotocin (NSC-37917) rendered diabetic chinese hamsters. Ann Ophthalmol 1971;3:596–601.

Steffes MW, Mauer SM. Diabetic glomerulopathy in man and experimental animal models. Int Rev Exp Pathol 1984;26: 147–75.

Turk J, Corbett J A, Ramanadham S, Bohrer A, Mcdaniel ML. Biochemical evidence for nitric oxide formation from streptozotocin in isolated pancreatic islets. Biochem Biophys Res Commun 1993;197:1458–64.

Wang K, Shindoh H, Inoue T, Horii I. Advantages of in vitro cytotoxicity testing by using primary rat hepatocytes in comparison with established cell lines. J Toxicol Sci 2002;27:229–37.

ELSEVIER

Neurobiology of Disease

www.elsevier.com/locate/ynbdi
Neurobiology of Disease 18 (2005) 218–225

Ethylnitrosourea induces neural progenitor cell apoptosis after S-phase accumulation in a p53-dependent manner

Kei-ichi Katayama,* Masaki Ueno, Hirofumi Yamauchi, Takayuki Nagata, Hiroyuki Nakayama, and Kunio Doi

Department of Veterinary Pathology, Graduate School of Agricultural and Life Sciences, The University of Tokyo, Bunkyo-ku, Tokyo 113-8657, Japan

Received 10 April 2004; revised 8 September 2004; accepted 29 September 2004
Available online 2 December 2004

Neural progenitor cells populate the ventricular zone of the fetal central nervous system. In this study, immediately after the administration of ethylnitrosourea (ENU), an alkylating agent, an accumulation of neural progenitor cells in the S phase was observed. This event was caused by the inhibition or arrest of DNA replication rather than acceleration of the G1/S transition. Soon after this accumulation reached its peak, the number of cells in the G2/M phase decreased and the apoptotic cell count increased. In p53-deficient mice, both ENU-induced apoptosis and S-phase accumulation were almost completely abrogated. These findings indicate that ENU inhibits or arrests DNA replication in neural progenitor cells during the S phase and then evokes apoptosis before the cells enter the G2 phase. Furthermore, these data also demonstrate that both ENU-induced apoptosis and cell cycle perturbation in the S phase require p53.

Keywords: Apoptosis; Cell cycle arrest; Development; DNA damage; DNA replication; Ethylnitrosourea; Neural progenitor cell; p53

Introduction

In the fetal central nervous system (CNS), neural progenitor cells (NPCs) constitute a pseudostratified epithelium called the ventricular zone. NPCs are pluripotent cells that can self-renew and differentiate into cells of both the neuronal and glial lineage. In the ventricular zone, the nuclei of the NPCs undergo a series of characteristic movements called "elevator movements," and their locations are well correlated with the phase of the cell cycle. The nuclei of S-phase cells occupy the outer part of the ventricular zone. During the G2 phase, the nuclei move toward the ventricular surface, where the cells enter the M phase and complete mitosis. Nuclei of daughter cells that enter the G1 phase move outward, and then enter the S phase again in the outer part of the ventricular zone. In this way, NPCs proliferate and increase in number. During neurogenesis, after a division, one daughter cell differentiates into a neuroblast, escapes from the elevator movements, and migrates to the outside of the ventricular zone, where postmitotic neurons accumulate and form the cerebral neocortex (Yoshikawa, 2000).

Apoptosis is controlled by various signals during CNS development, and its precise regulation is indispensable for sound development (Oppenheim, 1991; Roth and D'Sa-Eipper, 2001). However, NPCs are quite susceptible to various types of stimuli, especially DNA-damaging agents, and easily enter the process of apoptotic cell death (D'Sa-Eipper and Roth, 2000; Kameyama and Inouye, 1994; Katayama et al., 2001). As a result of inappropriate apoptosis, congenital anomalies such as microencephaly, anencephaly, and cellular cytoarchitectural abnormalities may be induced in neonates (Katayama et al., 2000; Miki et al., 1995).

The tumor suppressor p53 has been implicated in cellular responses to DNA-damaging agents. In response to DNA damage, p53 is upregulated and transactivates a series of genes involved in the induction of apoptosis, cell cycle arrest, and DNA repair (Ko and Prives, 1996). NPC apoptosis induced by DNA-damaging agents is also mediated by the regulation of p53 and p53 target genes (Bolaris et al., 2001; Borovitskaya et al., 1996; Katayama et al., 2002; Ueno et al., 2002) and is efficiently inhibited in p53 knockout mice (D'Sa-Eipper et al., 2001; Kubota et al., 2000; Leonard et al., 2001).

Ethylnitrosourea (ENU) is a monofunctional alkylating agent with high mutagenicity (Shibuya and Morimoto, 1993). ENU selectively induces brain tumors in offspring when administered to pregnant animals, and this experimental model has been extensively used to investigate the pathogenesis of CNS tumors (Jang et al., 2004; Koestner, 1990). Most of the ENU-induced CNS tumors are regarded as gliomas, and the rat is the species most susceptible to neurogenic tumor development following ENU administration.

* Corresponding author. Department of Veterinary Pathology, Graduate School of Agricultural and Life Sciences, The University of Tokyo, 1-1-1 Yayoi, Bunkyo-ku, Tokyo 113-8657, Japan. Fax: +81 3 5841 8185.
E-mail address: katayama-vet@umin.ac.jp (K. Katayama).
Available online on ScienceDirect (www.sciencedirect.com).

0969-9961/$ - see front matter © 2004 Elsevier Inc. All rights reserved.
doi:10.1016/j.nbd.2004.09.015

In the present study, we investigated the relationship between apoptosis and the cell cycle in the fetal CNS after the administration of ENU to find out how fetal NPCs regulate the cell cycle and apoptosis and how they respond to DNA-damaging agents. Our findings indicate that ENU inhibits or arrests DNA replication in NPCs in the S phase and evokes apoptosis before the cells enter the G2 phase. Furthermore, our findings also demonstrate that ENU-induced apoptosis and cell cycle perturbation in the S phase both require p53.

Materials and methods

All procedures were performed in accordance with the protocol approved by the Animal Care and Use Committee of the Graduate School of Agricultural and Life Sciences, The University of Tokyo.

Chemicals

ENU, bromodeoxyuridine (BrdU), propidium iodide (PI), and RNaseA were obtained from Sigma (St. Louis, MO).

Animals

Pregnant F344 rats (plug day: day 0 of gestation) were obtained from Saitama Experimental Animal Company (Saitama, Japan), and pregnant ICR mice (plug day: day 0 of gestation) were purchased from Charles River Japan, Inc. (Kanagawa, Japan). $p53^{+/-}$ mice were purchased from Taconic (Germantown, NY). Heterozygous mice were crossed to generate wild-type, heterozygous, and homozygous gene-disrupted mice. Endogenous and disrupted genes were detected by polymerase chain reaction analysis of tail DNA extracts as described by Timme and Thompson (1994). Fas/CD95-mutant C57BL/6J-*lpr/lpr* mice and wild-type C57BL/6J mice were purchased from Japan SLC (Shizuoka, Japan). Fas/CD95-deficient fetuses were generated by crossing *lpr/lpr* mice, and wild-type fetuses were obtained by crossing wild-type mice.

Treatments for F344 rats and ICR mice

Pregnant animals were injected intraperitoneally (i.p.) with 60 mg/kg of ENU or an equivalent volume of buffer alone on day 11 (mice) or 13 (rats) of gestation, and fetuses were harvested at specific times after the treatment described in the text. Collected fetuses were subjected to histopathological examination, cell cycle analysis by flow cytometry, and Western blot analysis. For the histopathological analysis, fetuses were fixed in 10% neutral-buffered formalin and embedded in paraffin. Paraffin sections (4 μm) were stained with hematoxylin and eosin. Some of the sections were subjected to immunohistochemical staining for cleaved caspase-3 as mentioned below.

Treatments for p53 knockout and lpr/lpr mice

Pregnant mice were injected i.p. with 60 mg/kg of ENU on day 11 of gestation; dams were euthanized and fetuses were collected at 6 and 12 h after the treatment, respectively. As a control, dams were injected i.p. with an equivalent volume of buffer alone on day 11 of gestation and euthanized at 6 h after the treatment. Collected fetuses were subjected to histopathological examination and cell cycle analysis.

Cell cycle analysis

The fetal telencephalon was dissected in Hanks' balanced salt solution (HBSS) and dissociated by brief mechanical trituration in HBSS. Isolated cells were washed with phosphate-buffered saline (PBS) and fixed in 70% ethanol. Cells were then washed with PBS, incubated in PBS containing RNaseA, and stained with PI. Cell cycle phase analysis was performed using a FACScan (Becton-Dickinson, San Jose, CA). Ten thousand cells were examined in each sample. Using the Cell Quest program (Becton-Dickinson), doublets and debris were discarded and then percentages of cells in the various phases of the cell cycle were calculated.

BrdU-incorporation assay

To analyze the DNA-replicating cells by flow cytometry, a BrdU incorporation assay was performed on the rat fetuses collected at 6 h after the ENU treatment. Pregnant dams were injected i.p. with 20 mg/kg of BrdU exactly 1 h before euthanasia. Cells were isolated from the fetal telencephalon, washed with PBS, and fixed in 70% ethanol. After being washed with PBS, the cells were resuspended in 2 M HCl containing 0.5% Triton X-100. The cells were neutralized in 0.1 M $Na_2B_4O_7$ and then incubated with fluorescein isothiocyanate (FITC)-labeled anti-BrdU monoclonal antibody (Pharmingen, San Diego, CA). Then, they were resuspended in PBS containing PI and analyzed using a FACScan (Becton-Dickinson). Ten thousand cells were examined in each sample. By using the Cell Quest program (Becton-Dickinson), doublets and debris were discarded, and then percentages of cells in the various phases of the cell cycle and FITC (BrdU)-positive cells were calculated.

Histological observation of the migration of BrdU-incorporated NPC nuclei

To analyze the migration of NPC nuclei histologically, ICR mice were injected i.p. with 60 mg/kg of ENU or an equivalent volume of buffer alone on day 11 of gestation. Dams were administered i.p. with 20 mg/kg of BrdU 3 h after the ENU treatment. Then, fetuses were collected at 1, 3, 6, and 9 h after the BrdU administration (i.e., 4, 6, 9, and 12 h after the ENU treatment). Collected fetuses were fixed in 10% neutral-buffered formalin and embedded in paraffin. The paraffin sections were subjected to immunohistochemical staining for BrdU as described below.

Immunohistochemistry

Immunohistochemical staining for cleaved caspase-3 and BrdU was carried out by the labeled streptavidin biotin (LSAB) method with streptavidin (Dako, Carpinteria, CA). Rabbit anti-cleaved caspase-3 polyclonal antibody (Cell Signaling Technology, Beverly, MA) and mouse anti-BrdU monoclonal antibody (Dako) were used as the primary antibodies. The positive signals were visualized using a peroxidase-diaminobenzidine reaction, and then the sections were counterstained with methyl green.

Western blot analysis

The fetal telencephalon was homogenized in a solution of 20 mM Tris–HCl (pH 7.4), containing 150 mM NaCl, 1 mM PMSF,

1% aprotinin, 2 mM EDTA, 2 mM Na_3VO_4, 1% NP-40, 0.1% SDS, and 1 mM DTT and centrifuged at 12,000 g for 20 min at 4°C. Approximately 30 μg of extract was loaded onto a 10% SDS-PAGE gel, electrophoresed, and transferred to a PVDF membrane (Bio-Rad, Hercules, CA). Blots were first probed with antibodies to p53 (Santa Cruz Biotechnology, Santa Cruz, CA), $p21^{waf1/cip1}$ (Pharmingen), cyclin D1 (Dako), cyclin-dependent kinase (CDK) 4 (Santa Cruz Biotechnology), and β-actin (Sigma). After incubation with the appropriate secondary antibody conjugated to horseradish peroxidase (Amersham, Buckinghamshire, UK), detection was performed with the ECL Plus kit (Amersham).

Results

ENU induces apoptosis in NPCs

In both rats and mice, an increase in the number of pyknotic cells, which fulfilled the morphological characteristics of apoptotic cells (Katayama et al., 2001), was observed from 3 to 24 h after the ENU treatment in the NPCs in the ventricular zone (Figs. 1a, b). Few pyknotic cells were observed in other zones. The nuclei of the pyknotic NPCs localized mainly in the outer part of the ventricular zone, which contains S-phase nuclei owing to the elevator movements. Immunohistochemically, pyknotic NPCs were also positively stained for cleaved caspase-3 (Figs. 1c, d), which is known to be involved in neural cell apoptosis during development as well as the apoptosis of neurons induced by DNA-damaging agents (Kuida et al., 1996; Keramaris et al., 2000).

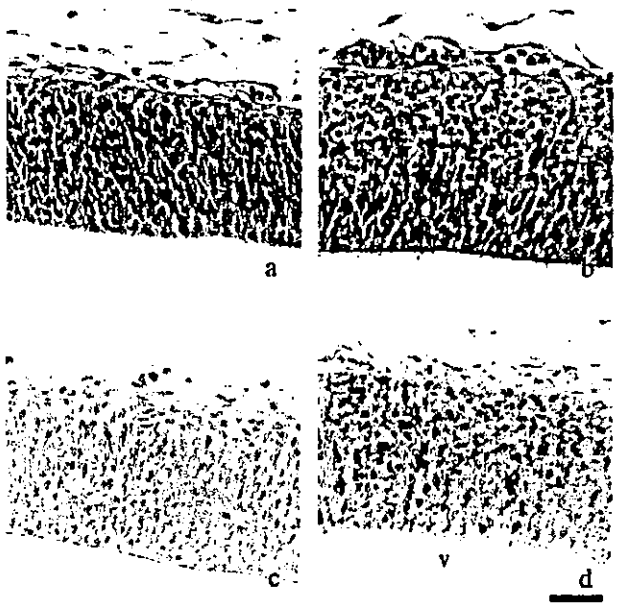

Fig. 1. ENU induces apoptosis and caspase-3 activation in NPCs in the fetal CNS. Transverse sections of the telencephalon at 12 h after the treatment. Hematoxylin and eosin-stained sections of the control (a) and ENU-treated (b) rat fetuses. Apoptotic NPCs bearing pyknotic nuclei are seen in the ENU-treated fetus. Apoptotic nuclei mainly localize in the outer part of the ventricular zone. Immunohistochemistry for cleaved caspase-3 of the control (c) and ENU-treated (d) rat fetuses. Extensive caspase-3 activation, as indicated by cleaved caspase-3 immunoreactivity, is observed in the ENU-treated fetus. V, ventricle; scale bar = 30 μm.

ENU induces S-phase accumulation in NPCs

Studies have shown that from gestational day 12 to 13, about 70% of mouse telencephalic cells are NPCs (D'Sa-Eipper and Roth, 2000); therefore, the results from our flow cytometric analyses are considered to accurately represent the cell cycle changes in NPCs. In both rats and mice, an accumulation of cells in the S phase was observed from 1 h after the ENU treatment, and this became most prominent at 6 h (Figs. 2, 3). Although the number of cells in S phase gradually decreased from 9 to 12 h, the number in G2/M phase also decreased at these time points. Furthermore, apoptotic cells (cells with sub-G1 DNA content) peaked at 12 h. The number of cells in G0/G1 phase decreased markedly between 6 and 12 h. The DNA content of the accumulated S-phase cells was close to that of the G1 cells, and it did not tend to increase with time (Fig. 2).

ENU inhibits or arrests DNA replication in NPCs

In our previous study, immunohistochemical staining for BrdU revealed a significant decrease in the number of BrdU-incorporated NPCs (DNA-replicating NPCs) in the fetal telencephalon after ENU administration, with a trough observed at 6 h (Katayama et al., 2001). Oyanagi et al. (1998) also reported that the number of BrdU-incorporated NPCs decreased immediately after the administration of ENU. However, in the present study, an accumulation of cells in the S phase was observed, and it became most prominent at 6 h after the ENU treatment. Therefore, we tried to analyze BrdU incorporation by flow cytometry.

At 6 h after the ENU treatment, BrdU incorporation in the fetal telencephalon was markedly reduced, as indicated by the decrease in FITC fluorescence intensity (Fig. 4). The number of BrdU-positive cells also decreased (mean ± standard deviation, control: 23.0 ± 1.6%, $n = 3$; ENU: 18.6 ± 1.0%, $n = 3$). In addition, there were many cells that contained DNA identical to that of the S-phase cells but did not incorporate BrdU (control: 0.9 ± 0.1%, $n = 3$; ENU: 15.2 ± 1.5%, $n = 3$). The DNA content of these cells was close to that of the G1 cells and identical to that of the accumulated S-phase cells observed in the cell cycle analysis. Almost the same results were obtained from mouse fetuses (data not shown). The results from the BrdU-incorporation assay suggest that S-phase accumulation is not brought about by acceleration of the G1/S transition but by the inhibition or arrest of DNA replication.

Migration of NPC nuclei is inhibited by ENU administration

To further analyze the cell cycle perturbation, we injected BrdU into pregnant mice at 3 h after the ENU treatment, when the accumulation of cells in the S phase began to be apparent, and analyzed the migration of BrdU-incorporated nuclei immunohistochemically. In both the control and ENU-treated fetuses, at 1 h after the BrdU administration, BrdU-incorporated NPC nuclei localized in the outer part of the ventricular zone, which contains S-phase nuclei owing to the elevator movements. In the control fetuses, BrdU-incorporated nuclei migrated toward the ventricular surface and showed mitotic figures from 3 to 6 h, and at 9 h, they began to move outward (Fig. 5). This result agrees well with the study of Takahashi et al. (1993), who reported that the S, G2/M, and G1 phases in mouse NPCs lasted 3.8, 2, and 9.3 h, respectively. In the ENU-treated fetuses, however, a large number of the BrdU-incorporated nuclei remained in the outer part of the

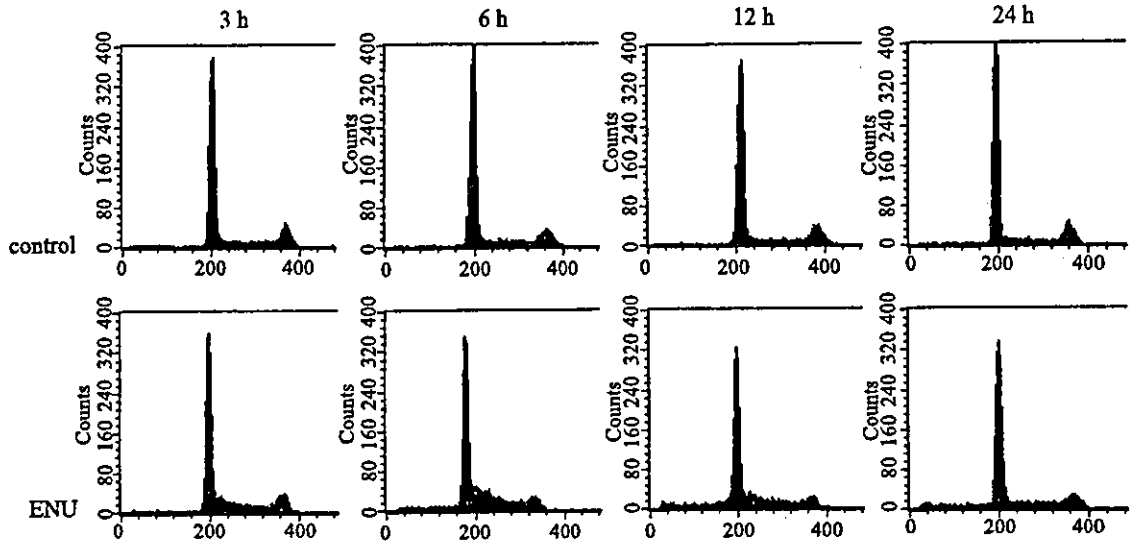

Fig. 2. ENU induces S-phase accumulation before the induction of apoptosis. Flow cytometric analysis of cells from rat fetal telencephalon. Horizontal and vertical axes represent PI fluorescence (DNA content) and cell number, respectively. S-phase accumulation was observed in the ENU-treated telencephalic cells and was most prominent at 6 h after the treatment. The number of cells in the G2/M phase decreased and that of apoptotic cells (cells with sub-G1 DNA content) increased at 12 h. The DNA content of the accumulated S-phase cells was close to that of the G1 cells and did not tend to increase with time.

ventricular zone from 3 to 6 h, finally reaching the ventricular surface at 9 h (Fig. 5). In addition, pyknotic nuclei positively stained by the anti-BrdU antibody were observed from 3 to 9 h after the BrdU administration, and these nuclei were mainly observed in the outer part of the ventricular zone; as a result, BrdU-positive nuclei markedly decreased at 9 h. These findings indicate that BrdU-incorporated NPC nuclei remain in the outer part of the ventricular zone for a long time and appear pyknotic before they move inward. According to the elevator movements, the results suggest that ENU induces cell cycle retardation in NPCs in the S phase and apoptosis occurs while they are still in the S phase. We performed the same experiment in rat fetuses, but BrdU-positive signals were very weak in the ENU-treated fetuses, and it was difficult to evaluate the migration of BrdU-incorporated nuclei.

S-phase accumulation is not accompanied by elevated expression of cell cycle promoting molecules

The expression of proteins involved in the G1/S transition was analyzed by Western blot using protein samples extracted from rat telencephalon (Fig. 6; Sherr and Roberts, 1999). The expression of cyclin D1, which promotes G1/S transition, decreased from 3 h after the ENU treatment. However, the expression of $p21^{waf1/cip1}$, a CDK inhibitor, increased at around 6 h, and the expression of p53, a transcriptional regulator of $p21^{waf1/cip1}$, also increased and peaked at 3 h. In our previous study, elevation in the levels of p53 and $p21^{waf1/cip1}$ proteins was also detected by immunohistochemistry (Katayama et al., 2002). The expression of CDK4 was nearly unchanged throughout the experimental period. Almost the same results were obtained from mouse fetuses (data not shown).

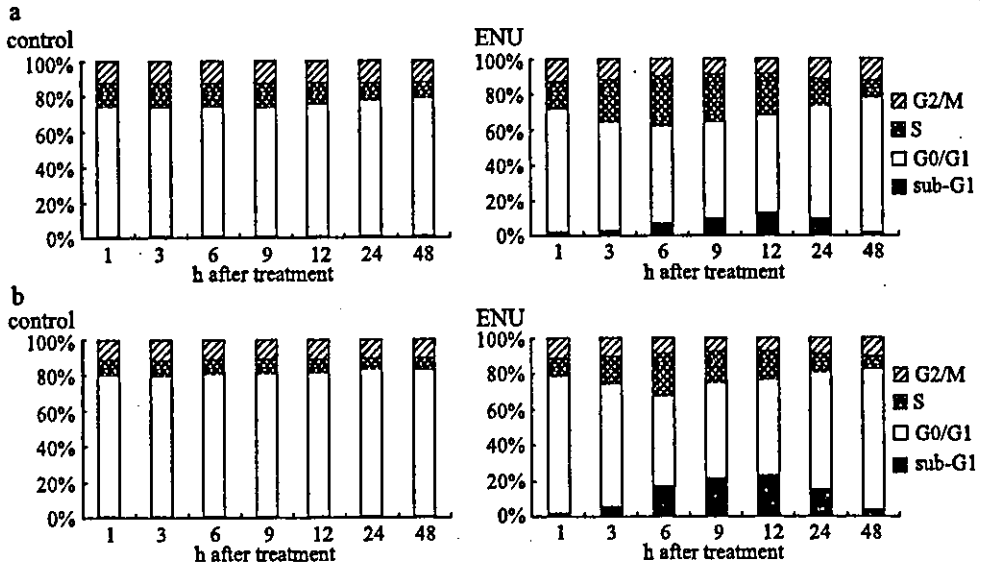

Fig. 3. Cell cycle distribution of control and ENU-treated rat (a) and mouse (b) fetal telencephalic cells. Percentages for each cell cycle phase are presented as the mean of three dams.

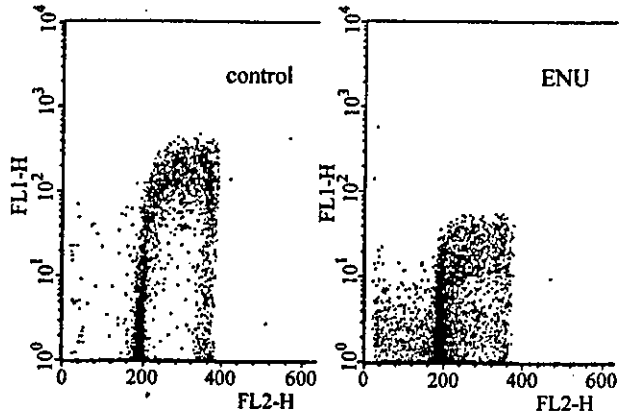

Fig. 4. ENU inhibits or arrests DNA replication in the telencephalic cells. Dot blots of cell cycle distribution and BrdU incorporation in rat fetal telencephalic cells. FITC-fluorescence (BrdU incorporation) on the vertical axis (log scale) and PI fluorescence (DNA content) on the horizontal axis. BrdU incorporation is severely inhibited in the ENU-treated fetus. In addition, there are many cells that contain DNA identical to that of the S-phase cells but do not incorporate BrdU.

These results also suggest that the accumulation of cells in the S phase is not brought about by the acceleration of the G1/S transition.

p53 is required for both ENU-induced apoptosis and S-phase accumulation

In the histopathology and cell cycle analysis of p53 knockout mice, we could not detect an increase in the number of apoptotic cells in the $p53^{-/-}$ mice after the administration of ENU (Figs. 7a, b, 8a). In addition, $p53^{-/-}$ mice showed almost no changes in the cell cycle distribution compared to the $p53^{+/+}$ and $p53^{+/-}$ mice (Fig. 8a). These findings suggest that p53 is required for both ENU-induced apoptosis and cell cycle perturbation in the S phase.

Fas/CD95 is not critical for ENU-induced apoptosis or S-phase accumulation

Fas/CD95 is a member of the tumor necrosis factor receptor superfamily and induces apoptosis when it binds to Fas/CD95 ligand (Itoh et al., 1991). Recent studies have indicated the involvement of the Fas/CD95 system in neuronal cell death in several neurological disorders (Hou et al., 2002; Padosch et al., 2003; Tan et al., 2001). Fas/CD95 is also known as a transcriptional target of p53 (Muller et al., 1998), and the expression of Fas/CD95 mRNA was upregulated after the activation of p53 in our previous study (Katayama et al., 2002). In *lpr/lpr* mice, which lack Fas/CD95 (Watanabe-Fukunaga et al., 1992), apoptosis and cell cycle perturbation were also observed upon administration of ENU, as in the wild-type C57BL/6J mice (Figs. 7c, d, 8b). Thus, Fas/CD95 is not critical for ENU-induced apoptosis or cell cycle alteration in the fetal CNS.

Discussion

In the present study, an accumulation of cells in the S phase was observed immediately after the administration of ENU. Our findings indicate that the accumulation is brought about by the inhibition or arrest of DNA replication rather than by the acceleration of the G1/S transition. Soon after the number of cells in the S phase reached its peak, the cells in the G2/M phase decreased and the number of apoptotic cells increased. In the p53-deficient mice, both ENU-induced NPC apoptosis and S-phase accumulation were almost completely abrogated. These findings indicate that ENU inhibits or arrests DNA replication in NPCs in the S phase and then signals for apoptosis before the cells enter the G2 phase. Furthermore, these data also demonstrate that both ENU-induced apoptosis and S-phase accumulation require p53.

After the administration of ENU to pregnant rats on day 15 of gestation, apoptotic cells were observed not only in the NPCs but also in the neuroblasts immediately after mitosis in the outside of

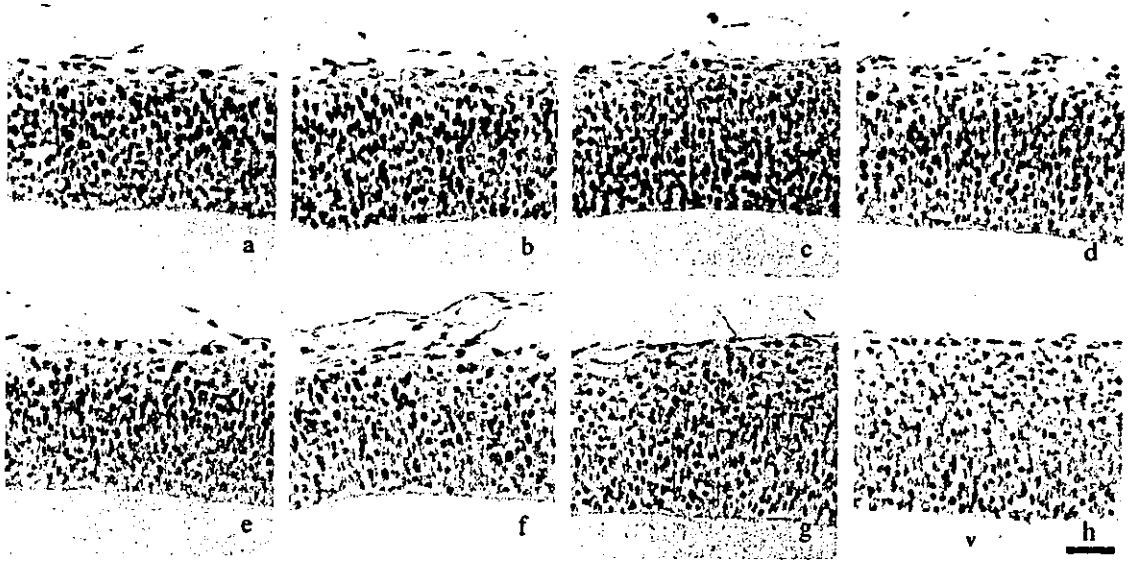

Fig. 5. Migration of BrdU-incorporated NPC nuclei is retarded by ENU administration. Immunohistochemistry for BrdU of the control (a–d) and ENU-treated (e–h) mouse fetal telencephalon at 1 (a, e), 3 (b, f), 6 (c, g), and 9 h (d, h) after the BrdU administration. The migration of BrdU-incorporated nuclei toward the ventricular surface is inhibited in the ENU-treated fetuses, indicating the cell cycle retardation in the S phase. In addition, some BrdU-positive nuclei remaining in the outer part of the ventricular zone appear pyknotic. V, ventricle; scale bar = 30 μm.

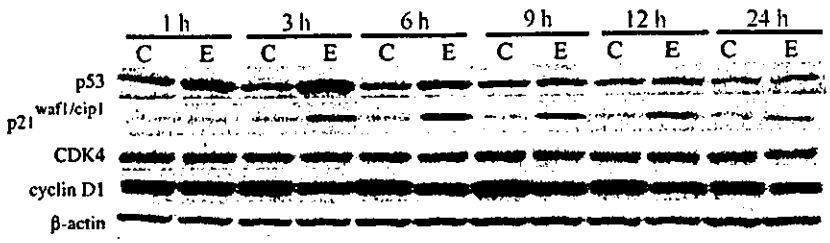

Fig. 6. Expression of cell cycle regulators during ENU-induced S-phase accumulation. Western blot analysis of p53, $p21^{waf1/cip1}$, CDK4, cyclin D1, and β-actin obtained from extracts from the control (C) and ENU-treated (E) rat telencephalon. The expression of p53 and $p21^{waf1/cip1}$ increased, cyclin D1 decreased, and CDK4 was unchanged in the ENU-treated fetuses.

the ventricular zone (Oyanagi et al., 1998). Day 15 of gestation in rats is the stage of neurogenesis. One NPC produces one neuroblast and one NPC by mitosis, and generated neuroblasts migrate to the outside of the ventricular zone. In the present experiment, at the time of the ENU administration (day 13 of gestation in rats and day 11 in mice), the fetal CNS was still undifferentiated, and consequently, the generation of neuroblasts was not very prominent. Thus, there was not marked apoptotic cell death in the neuroblasts in the present study. Although we cannot exclude the possibility that apoptosis is also induced in other ways, the results of this study strongly suggest that a large number of the NPCs die in the S phase after cell cycle retardation in the S phase.

ENU alkylates mainly the O^6 position of guanine (Shibuya and Morimoto, 1993), and the existence of alkyl lesions in the genomic DNA inhibits DNA replication in vitro (Ceccotti et al., 1993; Eckert et al., 1997). The retardation of the cells in S phase observed in the present study indicates that ENU also inhibits DNA replication in vivo. The O^6 alkylation of guanine induces GC-AT transitions. The brain eliminates O^6-alkylguanine at a much lower rate than other organs, and the long-term retention of O^6-alkylguanine in the brain is thought to be the cause of brain neoplasms (Koestner, 1990). Elimination of DNA-damaged cells by p53-dependent apoptosis is very important for the prevention of brain tumorigenesis (Leonard et al., 2001). However, it is still controversial that a high incidence of brain neoplasms is observed in rat neonates in spite of extensive apoptotic cell death in the fetal CNS after the administration of ENU.

Recent studies suggest the involvement of the cell cycle machinery of the G1/S transition such as activation of cyclin–CDK complexes, phosphorylation of retinoblastoma protein, and derepression of E2F-responsive genes in the postmitotic neuronal apoptosis induced by DNA damage (Liu and Greene, 2001;

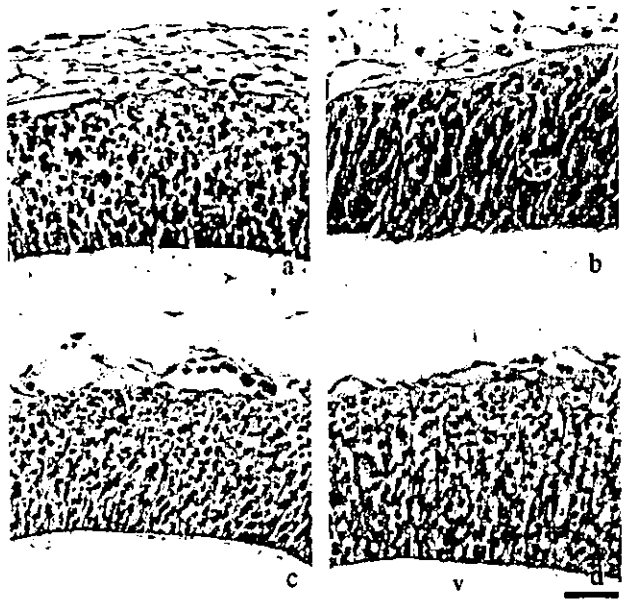

Fig. 7. p53, but not Fas/CD95, is required for ENU-induced NPC apoptosis. Hematoxylin and eosin-stained sections of the telencephalon from $p53^{+/+}$ (a), $p53^{-/-}$ (b), wild-type C57BL/6J (c), and *lpr/lpr* (d) mouse fetuses at 12 h after the ENU treatment. ENU-induced apoptotic cell death is almost completely abrogated in the p53-deficient mouse, and apoptosis is similarly induced in both the wild-type C57BL/6J and *lpr/lpr* mice. V, ventricle; scale bar = 30 μm.

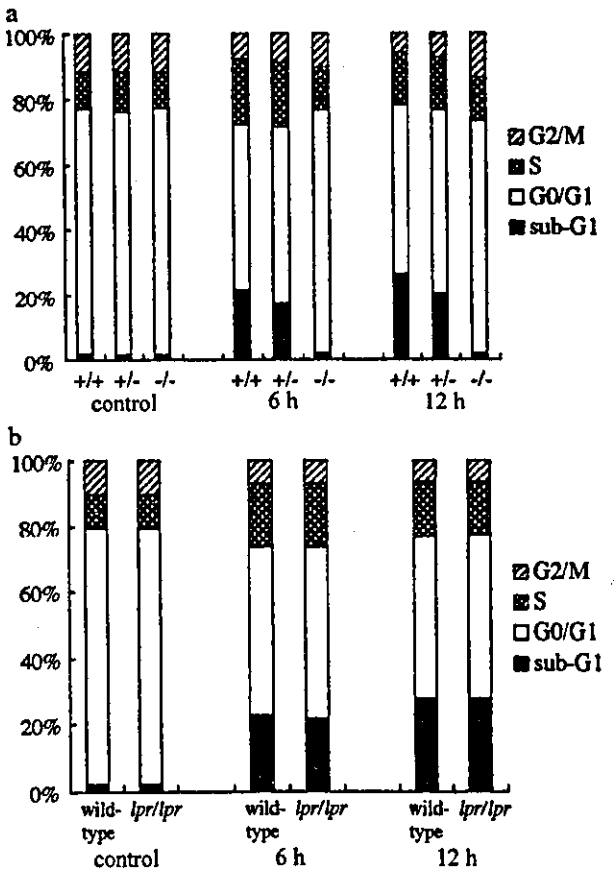

Fig. 8. Cell cycle distribution of p53 knockout (a) and *lpr/lpr* (b) mouse fetal telencephalic cells. Percentages for each cell cycle phase are presented as the mean of three dams. Both ENU-induced apoptosis and S-phase accumulation were almost completely abrogated in p53-deficient mice, and they were similarly induced in wild-type C57BL/6J and *lpr/lpr* mice.

Morris et al., 2001; Park et al., 1997, 1998, 2000). In the present study, the expression of cyclin D1 and CDK4 was not upregulated by ENU administration. Responses to DNA-damaging agents differ between postnatal and embryonic neurons (Johnson et al., 1999) and among embryonic neurons in various developmental stages (Lee et al., 2001). Thus, the findings of the present study would be a specific response of the fetal NPC, which are highly proliferative.

In the Western blot analysis, the expression of $p21^{waf1/cip1}$ was upregulated and peaked at around 6 h after the ENU treatment. Almost the same observation was made in an immunohistochemical analysis (Katayama et al., 2002). $p21^{waf1/cip1}$, a CDK inhibitor, is transactivated by p53 and induces cell cycle arrest in the G1 phase (Dulic et al., 1994; El-Deiry et al., 1993). We performed immunohistochemical staining for $p21^{waf1/cip1}$ in p53 knockout mice and found an increase in the number of $p21^{waf1/cip1}$-positive NPCs in the $p53^{+/+}$ and $p53^{+/-}$ mice, but not in the $p53^{-/-}$ mice after the administration of ENU (data not shown). This finding suggests that $p21^{waf1/cip1}$ is also upregulated in a p53-dependent manner. However, the number of cells in G0/G1 phase decreased and that in S phase increased on administration of ENU, indicating that the cell cycle is arrested in the S phase rather than in the G1 phase. Thus, the precise role of $p21^{waf1/cip1}$ is not clear. In our previous study, the number of $p21^{waf1/cip1}$-positive NPCs after ENU administration was much less than that of p53-positive cells (maximum index of $p21^{waf1/cip1}$ was about one fourth that of p53; Katayama et al., 2002); therefore, the fetal CNS would tend to eliminate DNA-damaged cells via apoptosis rather than arrest the cell cycle and repair the DNA lesions. Furthermore, the mechanism of the p53-dependent induction of the S-phase accumulation is not clear. Additional studies are needed to determine the key molecule required for the S-phase accumulation.

In the cell cycle analysis of p53 knockout mice, percentages of cells in the S phase at 6 and 12 h and G2/M phase at 12 h after the ENU treatment slightly increased in $p53^{-/-}$ mice. Though we cannot exclude the possibility that alkylation of the bases by ENU has some effect(s) on the cell cycle progression even in p53-deficient mice, the changes in the percentage of each cell cycle phase of $p53^{-/-}$ mice were not significantly different from the control ($P > 0.05$, Student's t test), whereas all the changes except G2/M phase of $p53^{+/-}$ mice at 6 h were significantly different in $p53^{+/+}$ and $p53^{+/-}$ mice ($P < 0.05$, Student's t test).

DNA damage-induced NPC apoptosis requires p53 and caspase-9 (D'Sa-Eipper et al., 2001; Leonard et al., 2001), and ataxia telangiectasia mutated (ATM) is required for the activation of p53 (Lee et al., 2001). However, little is known about how NPCs regulate apoptosis and the cell cycle. NPCs are highly proliferative and have the potential to differentiate into cells of both the neuronal and glial lineage. Thus, elucidating the mechanisms of how NPCs regulate the cell cycle and apoptosis and respond to exogenous stimuli is important for understanding both normal and abnormal development of the CNS.

Acknowledgment

This study was supported financially by the Japan Society for the Promotion of Science.

References

Bolaris, S., Bozas, A., Benekou, H., Philippidis, H., Stylianopoulou, F., 2001. In utero radiation-induced apoptosis and p53 gene expression in the developing rat brain. Int. J. Radiat. Biol. 77, 71–81.

Borovitskaya, A.E., Vladmir, I.E., Steven, L.S., 1996. Gamma-radiation-induced cell death in the fetal rat brain possesses molecular characteristics of apoptosis and is associated with specific messenger RNA elevations. Mol. Brain Res. 35, 19–30.

Ceccotti, S., Dogliotti, E., Gannon, J., Karran, P., Bignami, M., 1993. O^6-methylguanine in DNA inhibits replication in vitro by human cell extracts. Biochemistry 32, 13664–13672.

D'Sa-Eipper, C., Roth, K.A., 2000. Caspase regulation of neuronal progenitor cell apoptosis. Dev. Neurosci. 22, 116–124.

D'Sa-Eipper, C., Leonard, J.R., Putcha, G., Zheng, T.S., Flavell, R.A., Rakic, P., Kuida, K., Roth, K.A., 2001. DNA damage-induced neural precursor cell apoptosis requires p53 and caspase 9 but neither Bax nor caspase 3. Development 128, 137–146.

Dulic, V., Kaufmann, W.K., Wilson, S.J., Tlsty, T.D., Lees, E., Harper, J.W., Elledge, S.J., Reed, S.I., 1994. p53-dependent inhibition of cyclin-dependent kinase activities in human fibroblasts during radiation-induced G1 arrest. Cell 76, 1013–1023.

Eckert, K.A., Hile, S.E., Vargo, P.L., 1997. Development and use of an in vitro HSV-tk forward mutation assay to study eukaryotic DNA polymerase processing of DNA alkyl lesions. Nucleic Acids Res. 25, 1450–1457.

el-Deiry, W.S., Tokino, T., Velculescu, V.E., Levy, D.B., Parsons, R., Trent, J.M., Lin, D., Mercer, W.E., Kinzler, K.W., Vogelstein, B., 1993. WAF1, a potential mediator of p53 tumor suppression. Cell 75, 817–825.

Hou, S.T., Xie, X., Baggley, A., Park, D.S., Chen, G., Walker, T., 2002. Activation of the Rb/E2F1 pathway by the nonproliferative p38 MAPK during Fas (APO1/CD95)-mediated neuronal apoptosis. J. Biol. Chem. 277, 48764–48770.

Itoh, N., Yonehara, S., Ishii, A., Yonehara, M., Mizushima, S., Sameshima, M., Hase, A., Seto, Y., Nagata, S., 1991. The polypeptide encoded by the cDNA for human cell surface antigen Fas can mediate apoptosis. Cell 66, 233–243.

Jang, T., Litofsky, N.S., Smith, T.W., Ross, A.H., Recht, L.D., 2004. Aberrant nestin expression during ethylnitrosourea-(ENU)-induced neurocarcinogenesis. Neurobiol. Dis. 15, 544–552.

Johnson, M.D., Kinoshita, Y., Xiang, H., Ghatan, S., Morrison, R.S., 1999. Contribution of p53-dependent caspase activation to neuronal cell death declines with neuronal maturation. J. Neurosci. 19, 2996–3006.

Kameyama, Y., Inouye, M., 1994. Irradiation injury to the developing nervous system: mechanisms of neuronal injury. Neurotoxicology 15, 75–80.

Katayama, K., Ishigami, N., Suzuki, M., Ohtsuka, R., Kiatipattanasakul, W., Nakayama, H., Doi, K., 2000. Teratologic studies on rat perinates and offspring from dams treated with ethylnitrosourea (ENU). Exp. Anim. 49, 181–187.

Katayama, K., Uetsuka, K., Ishigami, N., Nakayama, H., Doi, K., 2001. Apoptotic cell death and cell proliferative activity in the rat fetal central nervous system from dams administered with ethylnitrosourea (ENU). Histol. Histopathol. 16, 79–85.

Katayama, K., Ohtsuka, R., Takai, H., Nakayama, H., Doi, K., 2002. Expression of p53 and its transcriptional target genes mRNAs in the ethylnitrosourea-induced apoptosis and cell cycle arrest in the fetal central nervous system. Histol. Histopathol. 17, 715–720.

Keramaris, E., Stefanis, L., MacLaurin, J., Harada, N., Takaku, K., Ishikawa, T., Taketo, M.M., Robertson, G.S., Nicholson, D.W., Slack, R.S., Park, D.S., 2000. Involvement of caspase 3 in apoptotic death of cortical neurons evoked by DNA damage. Mol. Cell. Neurosci. 15, 368–379.

Ko, L.J., Prives, C., 1996. p53: puzzle and paradigm. Genes Dev. 10, 1054–1072.

Koestner, A., 1990. Characterization of N-nitrosourea-induced tumors of the nervous system: their prospective value for studies of neurocarcinogenesis and brain tumor therapy. Toxicol. Pathol. 18, 186–192.

Kubota, Y., Takahashi, S., Sun, X.Z., Sato, H., Aizawa, S., Yoshida, K., 2000. Radiation-induced tissue abnormalities in fetal brain are related to apoptosis immediately after irradiation. Int. J. Radiat. Biol. 76, 649–659.

Kuida, K., Zheng, T.S., Na, S., Kuan, C., Yang, D., Karasuyama, H., Rakic, P., Flavell, R.A., 1996. Decreased apoptosis in the brain and premature lethality in CPP32-deficient mice. Nature 384, 368–372.

Lee, Y., Chong, M.J., McKinnon, P.J., 2001. Ataxia telangiectasia mutated-dependent apoptosis after genotoxic stress in the developing nervous system is determined by cellular differentiation status. J. Neurosci. 21, 6687–6693.

Leonard, J.R., D'Sa-Eipper, C., Klocke, B.J., Roth, K.A., 2001. Neural precursor cell apoptosis and glial tumorigenesis following transplacental ethyl-nitrosourea exposure. Oncogene 20, 8281–8286.

Liu, D.X., Greene, L.A., 2001. Regulation of neuronal survival and death by E2F-dependent gene repression and derepression. Neuron 32, 425–438.

Miki, T., Fukui, Y., Takeuchi, Y., Itoh, M., 1995. A quantitative study of the effects of prenatal X-irradiation on the development of cerebral cortex in rats. Neurosci. Res. 23, 241–247.

Morris, E.J., Keramaris, E., Rideout, H.J., Slack, R.S., Dyson, N.J., Stefanis, L., Park, D.S., 2001. Cyclin-dependent kinases and p53 pathways are activated independently and mediate Bax activation in neurons after DNA damage. J. Neurosci. 21, 5017–5026.

Muller, M., Wilder, S., Bannasch, D., Israeli, D., Lehlbach, K., Li-Weber, M., Friedman, S.L., Galle, P.R., Stremmel, W., Oren, M., Krammer, P.H., 1998. p53 activates the CD95 (APO-1/Fas) gene in response to DNA damage by anticancer drugs. J. Exp. Med. 188, 2033–2045.

Oppenheim, R.W., 1991. Cell death during development of the nervous system. Annu. Rev. Neurosci. 14, 453–501.

Oyanagi, K., Kakita, A., Yamada, M., Kawasaki, K., Hayashi, S., Ikuta, F., 1998. Process of repair in the neuroepithelium of developing rat brain during neurogenesis: chronological and quantitative observation of DNA-replicating cells. Brain Res. Dev. Brain Res. 108, 229–238.

Padosch, S.A., Popp, E., Vogel, P., Bottiger, B.W., 2003. Altered protein expression levels of Fas/CD95 and Fas ligand in differentially vulnerable brain areas in rats after global cerebral ischemia. Neurosci. Lett. 338, 247–251.

Park, D.S., Morris, E.J., Greene, L.A., Geller, H.M., 1997. G1/S cell cycle blockers and inhibitors of cyclin-dependent kinases suppress camptothecin-induced neuronal apoptosis. J. Neurosci. 17, 1256–1270.

Park, D.S., Morris, E.J., Padmanabhan, J., Shelanski, M.L., Geller, H.M., Greene, L.A., 1998. Cyclin-dependent kinases participate in death of neurons evoked by DNA-damaging agents. J. Cell Biol. 143, 457–467.

Park, D.S., Morris, E.J., Bremner, R., Keramaris, E., Padmanabhan, J., Rosenbaum, M., Shelanski, M.L., Geller, H.M., Greene, L.A., 2000. Involvement of retinoblastoma family members and E2F/DP complexes in the death of neurons evoked by DNA damage. J. Neurosci. 20, 3104–3114.

Roth, K.A., D'Sa-Eipper, C., 2001. Apoptosis and brain development. Ment. Retard. Dev. Disabil. Res. Rev. 7, 261–266.

Sherr, C.J., Roberts, J.M., 1999. CDK inhibitors: positive and negative regulators of G1-phase progression. Genes Dev. 13, 1501–1512.

Shibuya, T., Morimoto, K., 1993. A review of the genotoxicity of 1-ethyl-1-nitrosourea. Mutat. Res. 297, 3–38.

Takahashi, T., Nowakowski, R.S., Caviness Jr., V.S., 1993. Cell cycle parameters and patterns of nuclear movement in the neocortical proliferative zone of the fetal mouse. J. Neurosci. 13, 820–833.

Tan, Z., Levid, J., Schreiber, S.S., 2001. Increased expression of Fas (CD95/APO-1) in adult rat brain after kainate-induced seizures. NeuroReport 12, 1979–1982.

Timme, T.L., Thompson, T.C., 1994. Rapid allelotype analysis of p53 knockout mice. Biotechniques 17, 460–463.

Ueno, M., Katayama, K., Nakayama, H., Doi, K., 2002. Mechanisms of 5-azacytidine (5AzC)-induced toxicity in the rat foetal brain. Int. J. Exp. Pathol. 83, 139–150.

Watanabe-Fukunaga, R., Brannan, C.I., Copeland, N.G., Jenkins, N.A., Nagata, S., 1992. Lymphoproliferation disorder in mice explained by defects in Fas antigen that mediates apoptosis. Nature 356, 314–317.

Yoshikawa, K., 2000. Cell cycle regulators in neural stem cells and postmitotic neurons. Neurosci. Res. 37, 1–14.

Available online at www.sciencedirect.com

SCIENCE DIRECT

Experimental and Molecular Pathology 78 (2005) 64–70

Experimental and Molecular Pathology

www.elsevier.com/locate/yexmp

Effects of pregnancy on CYPs protein expression in rat liver

Xi Jun He, Noriko Ejiri, Hiroyuki Nakayama, Kunio Doi*

Department of Veterinary Pathology, Graduate School of Agricultural and Life Sciences, The University of Tokyo, Japan

Received 16 August 2004
Available online 2 November 2004

Abstract

A body of evidence suggests that pregnancy may be responsible for the depression in the microsomal enzyme activity and the reduction in the total content of cytochrome P450 (CYP) in the rat liver. However, changes in expression of individual CYP isozyme remain poorly known. The current study was designed to examine the changes in CYPs protein expression in the liver of F344 rats in midpregnancy and late pregnancy by Western blot analysis and immunohistochemistry. Total nine antirat CYPs antibodies (CYP1A1, CYP2B1/CYP2B2, CYP2C6, CYP2C12, CYP2D1, CYP2D4, CYP2E1, CYP3A1, and CYP4A1) were used. In comparison with age-matched nonpregnant control rats, there were significant decreases in hepatic levels of CYP2B2, CYP2C6, and CYP4A1 in midpregnancy (day 13) and CYP2B2, CYP2C6, CYP4A1, CYP1A1, CYP2B1, and CYP2E1 in late pregnancy (day 19). The expression of CYP2C12, CYP2D1, and CYP 3A1 did not differ between nonpregnant and pregnant rats, and CYP2D4 was not detectable in microsomal proteins obtained from nonpregnant and pregnant rats at a protein loading of 20 μg total protein per lane. Immunohistochemistry showed that there were no differences in the distribution and degree of immunostainability for the abovementioned antibodies to nine CYPs between pregnant and nonpregnant rats.

Keywords: CYPs; F344 rat; Immunohistochemistry; Pregnancy; Western blot analysis

Introduction

Cytochrome P450 isozymes (CYPs) are the collective term for a large superfamily of heme-containing proteins that play an important role in the oxidative metabolism of numerous endogenous and foreign compounds (Nelson et al., 1996). Four of the CYP450 families, families CYP1 to CYP4, defined on the basis of their amino acid sequence similarities, are involved in drug metabolism and are preferentially expressed in the liver.

Expression of CYPs is known to be influenced by a variety of endogenous and foreign factors such as inflammation, age, gender, nutritional status, pregnancy, and chemical exposure. Pregnancy is a physiological state accompanied by a high metabolic demand. This appears to be involved in changes in activity of hepatic cytochrome CYPs monooxygenase. Previous studies have demonstrated that normal pregnancy is associated with a decrease in total CYP450 content and/or reduced activity of microsomal drug-metabolizing enzyme in the liver (Dean and Stock, 1975, 1989; Feuer and Liscio, 1969; Guarino et al., 1969; Neale and Parke, 1973). Change in total CYP450 content or drug metabolism, however, does not reflect changes in expression of individual CYPs, because CYPs metabolize xenobiotics and endogenous substances with differing affinities; that is, each individual CYP is characterized by diverse substrate specificity and significant differences in regulation. Genetic variability among individual family members further contributes to significant intersubject differences in metabolic capacity and pharmacological response (Rogers et al., 2002). To date, only few individual CYPs have been investigated during pregnancy. The findings obtained in hamsters have shown that in comparison to nonpregnant controls, pregnant hamsters showed

* Corresponding author. Department of Veterinary Pathology, Graduate School of Agricultural and Life Sciences, The University of Tokyo, Yayoi 1-1-1, Bunkyo-ku, Tokyo 113-8657, Japan. Fax: +81 3 5841 8185.
E-mail address: akunio@mail.ecc.u-tokyo.ac.jp (K. Doi).

0014-4800/$ - see front matter © 2004 Elsevier Inc. All rights reserved.
doi:10.1016/j.yexmp.2004.08.011

markedly decreased hepatic levels of both CYP2E and CYP2B mRNAs, which correlated with the results seen in immunoblot studies for these isozymes (Miller et al., 1992). Borlakoglu et al. (1993) investigated the alterations in rat hepatic drug metabolism during pregnancy and lactation. In their data, Western blot analysis of microsomal proteins obtained from pregnant rats shows that the expression of CYP1A1, CYP1A2, CYP2A1, CYP2B1, and CYP4A1 was not detectable in pregnant rats at a protein loading at 3 μg total protein per well. Casazza et al. (1994) demonstrated that CYP2E1 expression is suppressed in females particularly in late pregnancy in both acetone-treated and untreated rats by using immunoblot and Northern blot analyses. In human, there is an increase in activity of CYP2C6 enzyme during pregnancy, as assessed with dextromethorphan phenotyping test (Wadelius et al., 1997). This has been thought to be due to an induction of CYP2C6 enzyme. In the study by Czekaj et al. (2000), pregnancy was associated with decreased levels of CYP2B1/CYP2B2 protein in the liver in control and tobacco smoke-treated rats. Recently, Ejiri et al. (2001, 2003) investigated the changes in the expression and localization of CYPs protein in rat placenta at 9, 11, 13, 16, and 19 days of gestation by Western blot analysis and immunohistochemical staining. Only CYP3A1 was clearly detected during a long period of pregnancy.

According to the above-cited studies, changes in expression of most hepatic CYPs during rat pregnancy remain poorly known. In the present study, a total of nine CYPs throughout CYP1 to CYP4 subfamilies were designed to investigate the changes in expression in midpregnancy (day 13) and late pregnancy (day 19) by using Western blot analysis. The nine CYPs are thought to be concerned with drug-metabolizing system. CYP1A1 is involved in the oxidation of a wide spectrum of endogenous compounds and xenobiotics; CYP2B1 and CYP2B2 are involved in the activation of arenes, arylamines, and nitrosamine; CYP2C metabolizes the endogenous compound, arachidonic acid, and as such may play an important physiological role via the generation of bioactive eicosanoids; CYP2D has been shown to be one of determinants of polymorphic drug oxidations in human and rats, and it mainly catalyzes reaction of debrisoquine 4-hydroxylation; CYP2E1 is the major component of the microsomal ethanol-oxidazing system (MEOS) and is responsible for the majority of acetone monooxygenase activity in rats; CYP3A catalyzes the 6β-hydroxylation of testosterone and metabolizes several drugs; CYP4A catalyzes the hydroxylation of the ω or ω-1 carbon of saturated and unsaturated fatty acids and prostaglandins.

In the present study, we also investigated the localization and distribution of these CYPs in the liver of pregnant and nonpregnant rats. The protocol of this study has been approved by the Animal Care and Use Committee of the Graduate School of Agricultural and Life Sciences, The University of Tokyo.

Materials and methods

Animals

Twelve pregnant and six age-matched nonpregnant female rats (11 weeks of age) were purchased from Saitama Experimental Animal Co. (Saitama, Japan) and used in this study. The day of a vaginal plug being recognized was designated as 0 day of gestation. The rats were individually housed in plastic cages in an animal room controlled at 23°C ± 2°C and at 55% ± 5% humidity condition with 14 h/10 h light/dark cycle, and fed pellets (MF, Oriental Yeast Co., Ltd., Tokyo, Japan) and water ad libitum. On days 13 and 19 of gestation, six dams were sacrificed. Livers were removed and used for Western blot analysis and immunohistochemical staining. Nonpregnant were used as controls.

Immunohistochemistry

Immunohistochemical staining for CYPs was carried out on the paraffin sections using a LSAB method with streptavidine (DAKO, Carpinteria, CA) (1:300). Monoclonal goat antirat CYP1A1, CYP2C6, CYP2E1, and CYP4A1 antibodies (Daiichi Pure Chemicals Co., Ltd., Tokyo, Japan) (1:200) and monoclonal rabbit antirat CYP2B1/2B2, CYP2C12, CYP2D1, CYP2D4, and CYP3A1 antibodies (Chemicon International Inc., Temecula, CA) (1:200) were used as the first antibody. Biotinylated antirabbit and antigoat antibodies (Kirkegaard and Perry Laboratories Inc., Gaithersburg, MD) (1:400) were used as the second antibody.

After having been deparaffinized, the sections were pretreated with trypsin solution (0.1% trypsin and 0.1% calcium chloride/Tris buffer) at 37°C for 30 min, then treated with 0.3% H_2O_2/methanol for 30 min to inactivate endogeneous peroxidase, and incubated in 8% skim milk/TBS at 37°C for 40 min to block nonspecific binding of the antibodies. The tissue sections were then incubated overnight at 4°C with the first antibodies diluted in 8% skim milk/TBS. Following washing in 3× TBS, the sections were incubated with the second antibodies for 30 min at room temperature and then in the streptavidine for 30 min. Finally, the sections were visualized by 0.05% 3,3′-diaminobenzidine (DAB) with 0.03% hydrogen peroxide in Tris HCl buffer, followed by counterstaining with methyl green.

Western blot analysis

Livers were homogenized in ice-cold 0.1 M phosphate buffer, pH 7.4, containing 150 mM KCl, 1 mM EDTA Na, and 1 mM DTT, and microsomes were prepared by differential centrifugation. Briefly, the liver homogenates were centrifuged at 9000 × *g* for 20 min at 4°C, and the resulting supernatant spun at 105,000 × *g* for 1 h at 4°C. After discarding the supernatant, the pellets were suspended in the same buffer and recentrifuged. The pellets were resuspended with 0.1 M PB, pH 7.4, containing 150 mM KCl, 20%

glycerol, 1 mM EDTA Na, and 1 mM DTT and stored at −80°C until used. Protein concentration of the samples was measured using bovine serum albumin (BSA) as the standard. Microsomal proteins (20 or 40 μl) were separated using SDS–PAGE in 10% polyacrylamide gels and electrophoretically transferred to polyvinylidene difluoride (PVDF) membrane (BIO-RAD, Richmond, CA), and the plate was blocked with 8% skim milk/TBS for 1 h at room temperature. The membrane was then incubated with the abovementioned antirat CYP1A1, CYP2B1/2B2, CYP2C6, CYP2C12, CYP2D1, CYP2D4, CYP2E1, CYP3A1, and CYP4A1 antibodies diluted in 8% skim milk/TBS (1:200) overnight at 4°C, followed by another 1-h incubation with horseradish peroxidase-conjugated secondary antibodies [donkey anti-rabbit IgG (Amersham Pharmacia Biotech Ltd., Arlington Heights, IL) and rabbit antigoat IgG (Cappel, Aurora, OH)]. The protein bands were visualized by ECL plus Western blotting detection system (Amersham Pharmacia Biotech Ltd.) followed by a brief exposure to Hyperfilm (Amersham Biosciences UK Ltd.). Quantity One v3.0 software (PDI, Inc., NY, USA) was used to quantitate the band intensities.

Statistical analysis

Results were presented as the mean ± standard deviation (SD). Student *t* test was employed to calculate the statistical significance between control and midpregnancy (day 13) or late pregnancy (day 19) groups.

Results

Change in body and liver weights

There were significant increases in the body and liver weights on day 19 of gestation (Table 1). On day 13 of gestation, there was no significant increase in the liver weight compared with nonpregnant controls, although there was a significant increase in maternal body weight (Table 1).

Findings of Western blot analysis

The results of Western blot analysis are shown in Figs. 1 and 2. The expression of CYP2C12, CYP2D1, and CYP 3A1 proteins did not differ between nonpregnant and pregnant (both days 13 and 19 of gestation) rats. CYP2D4

Table 1
Body and liver weights

Gestation day	Body weight (g)	Liver weight (g)
Nonpregnant	144.35 ± 3.72	5.69 ± 0.39
Day 13 of gestation	161.83 ± 5.94*	6.06 ± 0.35
Day 19 of gestation	201.13 ± 8.66**	8.91 ± 0.19**

Data are represented as mean ± SD of 6 rats.
* $P < 0.01$; significantly different from controls.
** $P < 0.001$ significantly different from controls.

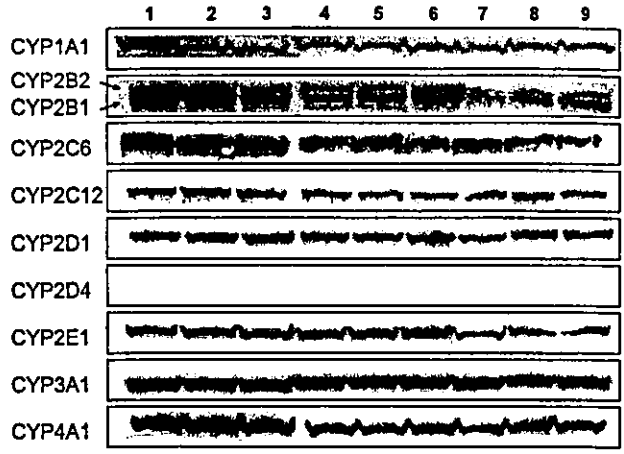

Fig. 1. Western blot analysis of liver microsomes from nonpregnant, midpregnant, and late pregnant rats. The amount of protein per lane was 20 μg (CYP2B1/2B2, CYP2C6 CYP2C12, CYP2D1, CYP2D4, CYP2E1, and CYP3A1) and 40 μg (CYP1A1 and CYP4A1). Lanes 1 to 3: Age-matched nonpregnant rats; lanes 4 to 6: midpregnant rats (day 13 of gestation); lanes 7 to 9: late pregnant rats (day 19 of gestation).

was not detectable in microsomal proteins obtained from nonpregnant and pregnant rats at a protein loading of 20 μg total protein per lane. Fig. 2 shows significant decreases in the CYP1A1, CYP2B1, and CYP2E1 contents in pregnant rats on day 19 of gestation (70.6%, 21.9%, and 61.0% of nonpregnant control values, respectively) and no significant change in pregnant rats on day 13 of gestation when compared with control. CYP2B2, CYP2C6, and CYP4A1 contents showed significant decreases on days 13 and 19 of gestation when compared with controls. Namely, on day 13 of gestation, CYP2B2, CYP2C6, and CYP4A1 proteins decreased to 29.2%, 67.4%, and 60.0% of control values, and on day 19 of gestation, they decreased to 25.8%, 69.8%, and 70.4% of control values, respectively.

Immunohistochemical findings

Immunohistochemical analysis with antibodies to CYPs revealed that CYP1A1 was expressed in endothelial cells of both sinusoids and veins in the liver (Figs. 3a–c) There was a very slight expression of CYP4A1 in hepatocytes and endothelial cells in the liver. CYP2C6 (Figs. 3d–f), CYP2E1 (Figs. 3g–i), CYP 3A1 (Figs. 3j–l), and other CYPs were mainly expressed in centrilobular hepatocytes. CYP2D4 was not detectable in either pregnant or nonpregnant rat liver by immunohistochemical analysis. As shown in Fig. 3, there were no differences in the distribution and degree of immunostainability for antibodies against nine CYPs between pregnant and nonpregnant rat livers. Table 2 shows the distribution and degree of immunostainability for nine CYPs.

Discussion

In the present study, in comparison to age-matched nonpregnant control rats, pregnant rats showed significantly

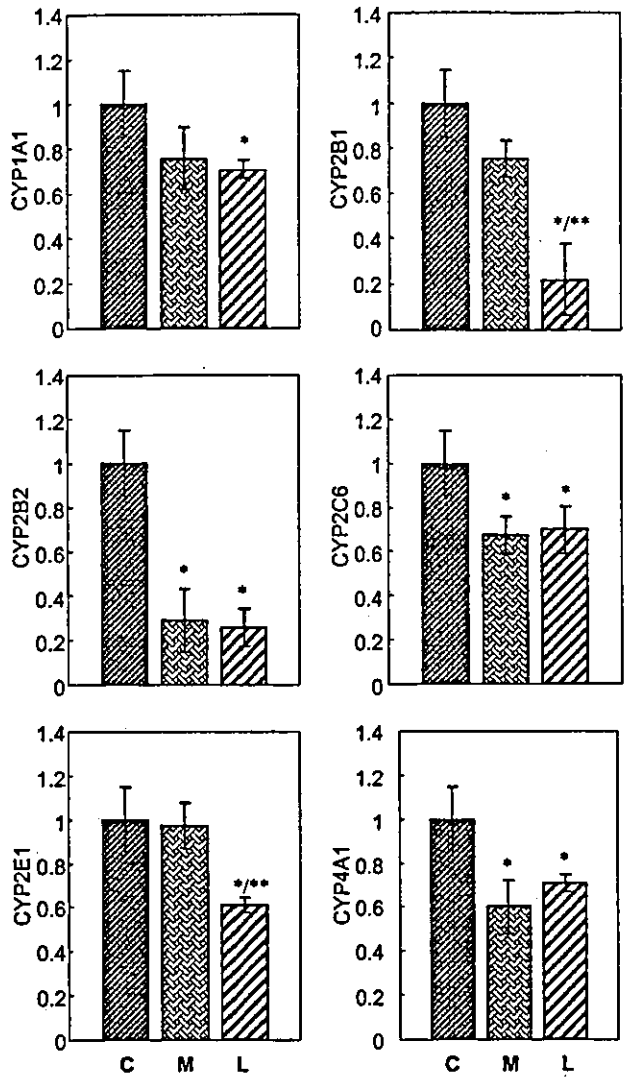

Fig. 2. Densitometry of Western blotting using monoclonal antibodies against rat hepatic CYP1A1, CYP2B1/2B2, CYP2C6, CYP2E1, and CYP4A1. Values are expressed as the ratio of pregnancy/nonpregnancy in arbitrary densitometric units of proteins amount and reported as the means ± SD of six rats. C indicates control nonpregnancy; M, midpregnancy; L, late pregnancy. *Significantly different from nonpregnant control at $P < 0.05$. **Significantly different from midpregnant rats at $P < 0.05$.

decreased hepatic levels of six out of nine CYPs proteins (CYP1A1, CYP2B1, CYP2B2, CYP2C6, CYP2E1, and CYP4A1) in midpregnancy (day 13) and/or late pregnancy (day 19).

Although, earlier reports have demonstrated that there was a decrease in rat hepatic total CYP450 content during pregnancy (Dean and Stock, 1975, 1989; Feuer and Kardish, 1975; Feuer and Liscio, 1969; Guarino et al., 1969), the mechanism of the effect of pregnancy on regulation of CYPs is still far from being fully clarified.

In the present study, pregnancy was linked to an increase in liver weight by up to 36.1% on day 19 of pregnancy. It has been hypothesized that a differential synthesis of hepatic proteins occurs during pregnancy, with little or no synthesis of the CYPs (Dean and Stock, 1975). It has also been thought that decrease in mixed-function oxidase activity during pregnancy is due to reduction in the hepatocellular capacity to metabolize drugs with an increase in liver size (Symons et al., 1982). However, in the present study, decreases in protein levels of CYPs (CYP2B2, CYP2C6, and CYP4A1) were not accompanied with an increase in liver weight, when detected in midpregnancy (day 13). Furthermore, Starkel et al. (2000) have demonstrated that early down-regulation of CYP3A and CYP2E1 in the regenerating rat liver is not related to the process of cellular proliferation. Therefore, liver enlargement might not be involved in the decrease in CYPs during rat pregnancy.

During pregnancy in rats, high plasma levels of both progesterone and its metabolites are produced. The depressed hepatic drug metabolism has been attributed to the pronounced hormonal changes that occur during pregnancy, in particular, to the higher plasma levels of both progesterone and its metabolites. Dean and Stock (1975) suggested that lower levels of hepatic microsomal enzyme activity might reflect a biological control mechanism to ensure the elevated levels of progesterone required to maintain the pregnant state. It has been known that the reduction in the activities of the microsomal drug-metabolizing enzymes in the rat is paralleled by a similar reduction in the total content of CYP450 (Dean and Stock, 1975; Feuer, 1979; Guarino et al., 1969; Neale and Parke, 1973). Thus, the increased production of progesterone and its metabolites can be implicated as a causative agent in pregnancy-induced regulation of CYPs; they seem to play a vital role in direct down-regulation of CYP450 expression and indirect reduction of the enzymatic activities.

Oxidative stress may be one of the factors which are responsible for the regulation of CYPs. In rats, lipid peroxidation remains low until midpregnancy and begins to rise after day 15 of pregnancy (Sugino et al., 1993). This role seems to be involved in our data; three out of nine CYPs decreased in midpregnancy (day 13), and up to six CYPs decreased in late pregnancy (day 19). Moreover, a measurable decrease in glutathione peroxidase in the liver and placenta, which play an important role in reducing the effects of oxidative stress in pregnancy, has been reported in pregnant rats (Mover-Lev and Ar, 1997). These observations indicate that there is an increase in oxidative stress during pregnancy. Oxidative stress has been suggested to result in the reduction of total CYP450 levels and drug metabolism activities in vivo (Gatti et al., 1993; Liu et al., 1993; Mannering and Deloria, 1986; Peristeris et al., 1992). Furthermore, Barker et al. (1994) have investigated the possibility that oxidative stress may influence inducer-dependent expression of CYP1A1 and CYP1A2, and demonstrated that hydrogen peroxide suppresses the accumulation of CYP1A1 and CYP1A2 mRNAs in isolated hepatocytes through a transcriptional mechanism. Pahan et al. (1997) demonstrated that there is a down-regulation of